AGU PUBLICATIONS

JGR

Journal of Geophysical Research: Atmospheres

RESEARCH ARTICLE
10.1002/2015JD024090

Key Points:
- New measurements of cloud droplet activation for strong nonionic surfactants
- CCN activity for Triton and Zonyl higher than predicted by partitioning theory
- CCN activity of internal mixtures is lower than predicted by ZSR mixing

Supporting Information:
- Tables S1–S3 and Captions of Data Sets S1–S22 and S23–31

Correspondence to:
M. D. Petters,
markus_petters@ncsu.edu

Citation:
Petters, S. S., and M. D. Petters (2016), Surfactant effect on cloud condensation nuclei for two-component internally mixed aerosols, *J. Geophys. Res. Atmos.*, *121*, 1878–1895, doi:10.1002/2015JD024090.

Received 13 AUG 2015
Accepted 27 JAN 2016
Accepted article online 29 JAN 2016
Published online 27 FEB 2016

©2016. American Geophysical Union. All Rights Reserved.

Surfactant effect on cloud condensation nuclei for two-component internally mixed aerosols

Sarah Suda Petters[1] and Markus Dirk Petters[1]

[1]Department of Marine, Earth, and Atmospheric Sciences, North Carolina State University at Raleigh, Raleigh, North Carolina, USA

Abstract This work presents experimental data on the cloud condensation nuclei (CCN) activity of two-component mixtures containing surfactants. Nine binary systems were tested combining strong ionic (sodium dodecyl sulfate) and nonionic surfactants (Zonyl FS-300 and Triton X-100) with nonsurfactant compounds (glucose, ammonium sulfate, or sodium chloride). Control tests were performed for systems combining organic (glucose) and inorganic compounds (ammonium sulfate or sodium chloride). Results show that CCN activity deviates strongly relative to predictions made from measurements of bulk surface tension. Köhler theory accounting for surface tension reduction and surface partitioning underpredicts the CCN activity of particles containing Zonyl FS-300 and Triton X-100. Partitioning theory better describes data for Zonyl FS-300 and Triton X-100 when limiting surface adsorption to 1.5 monolayers of the growing drop. Deviations from predictions were observed. Likely explanations include solute-solute interactions and nonspherical particle shape. The findings presented here examine in detail the perturbation of CCN activity by surfactants and may offer insight into both the success and limitations of physical models describing CCN activity of surface active molecules.

1. Introduction

Aerosols in the atmosphere are necessary precursors for cloud droplet formation. Variability in the relative abundance and effectiveness of cloud condensation nuclei (CCN) contributes to variability in the terrestrial radiative balance and water cycle [*Andreae and Rosenfeld*, 2008]. The current understanding of CCN thermodynamics is occluded in part by unresolved questions regarding the presence of surface active compounds in growing aqueous drops. Atmospheric aerosols and fog water extracts have been shown to reduce surface tension with respect to pure water [*Seidl and Hänel*, 1983; *Capel et al*., 1990; *Decesari et al*., 2000; *Facchini et al*., 2000]. By lowering tension at the air/water interface, surfactants decrease the energetic barrier to equilibrium droplet growth. However, migration of the surfactant from the interior of the droplet to the surface phase limits the number of moles of dissolved solute and thus reduces hygroscopic water uptake [*Sorjamaa et al*., 2004]. The treatment of surface tension reduction without accounting for the surfactant partitioning effect greatly exaggerates the potential of particles to nucleate cloud droplets [*Li et al*., 1998; *Sorjamaa et al*., 2004; *Prisle et al*., 2008]. Nevertheless, surfactants are often cited as cause for a discrepancy in CCN closure studies [*Moore et al*., 2008; *Engelhart et al*., 2008; *King et al*., 2009; *Wex et al*., 2009; *Padró et al*., 2010; *Giordano et al*., 2013], and surfactant partitioning is often not accounted for in studies highlighting the importance of surfactants in cloud activation processes [*Ekström et al*., 2009, 2010; *Padró et al*., 2010; *Giordano et al*., 2013; *Nozière et al*., 2014]. Perhaps, one reason for these citations is that CCN data demonstrating partitioning of surface active compounds are limited to a few systems. The main surfactants explored in previous studies have been sodium dodecyl sulfate and sodium fatty acid salts. Sufficient scatter in the published data makes rigorous validation of partitioning theory challenging. The aim of this work is to examine perturbations in CCN activity due to surfactants in sufficient detail to facilitate a discussion of physical mechanisms of surfactant action in CCN thermodynamics. We also discuss the diversity of surfactant types, the various mechanisms other than surface tension that alter CCN activity, and the limits imposed by experimental precision and model inputs.

2. Background

To motivate this study, we begin with a brief review of surfactants and their context in atmospheric aerosol. Figure 1 shows a survey of bulk surface tension data with respect to solution concentration for various surfactants (pastel colors, groups a–g). The groups, in order of their ability to reduce surface tension, are

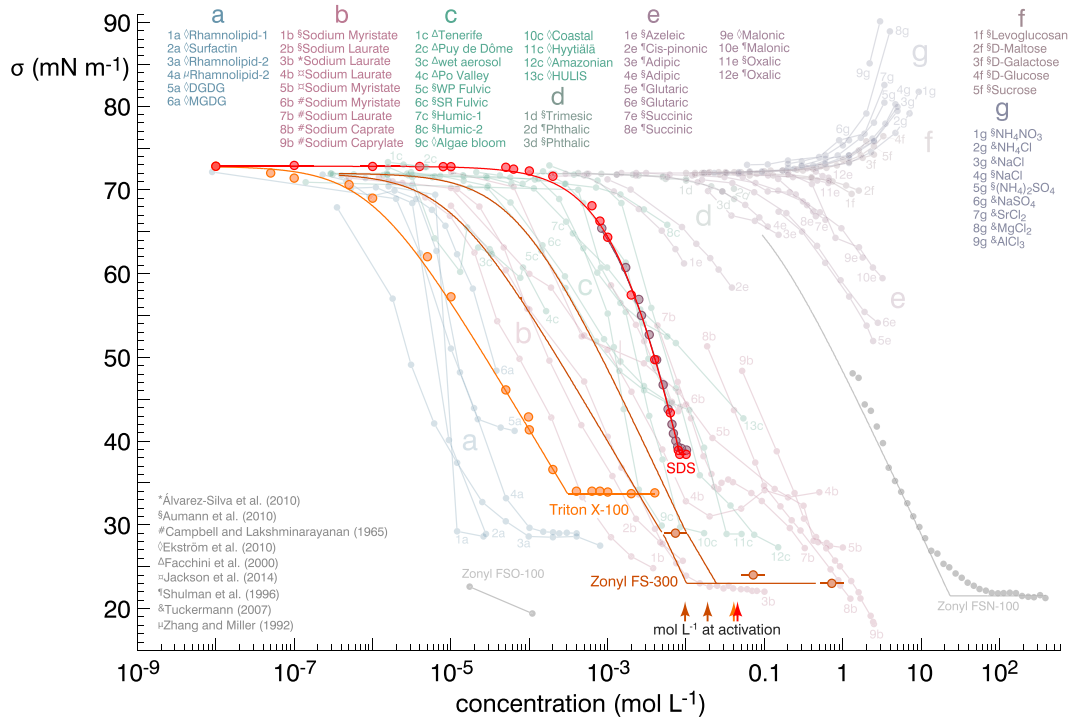

Figure 1. Szyszkowski curves. (foreground) Triton X-100 [*Zdziennicka et al*., 2012], Zonyl FS-300 [DuPont data sheet], Sodium dodecyl sulfate (SDS) (purple: *Rehfeld* [1967]; red: *Zdziennicka et al*. [2012]), Zonyl FSO-100 (grey: DuPont data sheet), and Zonyl FSN-100 (grey: *Škvarla et al*. [2014]). (background) Each trace has a number and letter corresponding to groups indicated above the data. Groups are (a) biosurfactants (DGDG is digalactosyl diacylglyceride; MGDG is monogalactosyl diacylglyceride), (b) fatty acid sodium salts, (c) ambient samples (WP is Waskish Peat; SR is Suwannee River; all assume molar mass of Fulvic Acid), (d) aromatic dicarboxylic and tricarboxylic acids, (e) organic acids, (f) saccharides, and (g) inorganic salts. Superscripts associated with sample names refer to the references included in the bottom left corner.

(a) biosurfactants, (b) fatty acid sodium salts, (c) ambient aerosol samples, (d) aromatic dicarboxylic and tricarboxylic acids, (e) nonaromatic organic acids, (f) saccharides, and (g) inorganic salts. Saccharides and inorganic salts increase surface tension for concentrated solutions and are included for completeness. In the foreground are sodium dodecyl sulfate (SDS; red and purple), Triton X-100 (orange), and fluorosurfactant Zonyl FS-300 (brown), which are investigated in this study. Figure 1 shows that the strongest surfactants begin reducing surface tension at concentration $> \sim 10^{-6}$ mol L^{-1}. For reference, classical Köhler theory [*Seinfeld and Pandis*, 2006] predicts that the solute concentration of single component particles at the point of activation ranges between 10^{-3} and 5×10^{-2} mol L^{-1} (assuming ideal solution behavior, surface tension of pure water at $T = 298$ K and evaluating the water content at activation for a plausible range of solute molecular weights $0.05 < M_s < 1$ kg mol^{-1}, solute density $700 < \rho_s < 2000$ kg m^{-3}, and solute dry diameter $50 < D_d < 200$ nm), implying that most compounds from groups (a–d) are strong enough surfactants to reduce the surface tension at the water content expected for activating cloud drops.

Ekström et al. [2009, 2010] suggest based on surface tension measurements and model calculations that biosurfactants lead to exceptional cloud nucleating efficiency. However, the authors did not directly measure CCN activity to confirm this hypothesis. Biosurfactants are surface-active molecules secreted by bacteria and are the strongest naturally occurring surfactants known (Figure 1, group a). Although whole bacteria are not considered to contribute strongly to CCN concentrations [*Sun and Ariya*, 2006; *Spracklen and Heald*, 2014], they are abundant in the atmosphere [*Burrows et al*., 2009] and are able to complete their life cycle in cloud water [*Sattler et al*., 2001]. Living bacteria or bacterial surfactants can be lofted into the air through wind action, wave breaking, or other mechanical means. The exceptionally small concentrations required for strong surface tension reduction by rhamnolipids (from *Pseudomonas aeruginosa*) [*Zhang and Miller*, 1992; *Ekström et al*., 2010] and surfactins (from *Bacillus subtilis*) [*Ekström et al*., 2010] may affect

21698996, 2016, 4, Downloaded from https://agupubs.onlinelibrary.wiley.com/doi/10.1002/2015JD024090 by University Of California, Wiley Online Library on [01/07/2024]. See the Terms and Conditions (https://onlinelibrary.wiley.com/terms-and-conditions) on Wiley Online Library for rules of use; OA articles are governed by the applicable Creative Commons License

CCN activation more than the nominally weaker surfactants. To our knowledge, no CCN data of these strong surfactants are available to date.

The fatty acid sodium salts in group (b) are strong surfactants of the formula $CH_3(CH_2)_xCOONa$, which have been used as model linear ionic surfactants for CCN studies [*Prisle et al*., 2008, 2010]. Furthermore, long-chain C_{13}–C_{30} carboxylic acids have been detected in ambient aerosol [*Mochida et al*., 2007; *Ho et al*., 2015] and have similar molecular form and surface tension reducing potential to their sodium salt counterparts [*Lunkenheimer et al*., 2003]. Fatty acid salts are anionic, and their dissolved ions may participate in counter ion interactions with other ionic species, affecting their solubility. Nonionic fatty acid counterparts may be salted out of solution in the presence of ions. The scatter in surface tensions of fatty acid sodium salts is large, possibly due to salting out effects, solution impurities, or other factors such as pH that either limit solubility or are impacted by low solubility. Some authors purified the samples by crystallization and filtration [*Zdziennicka et al*., 2012], whereas others did not [*Campbell and Lakshminarayanan*, 1965]. *Jackson et al*. [2014] note that sodium myristate (C_{14}) begins to precipitate at concentrations slightly above about 10^{-3} mol L^{-1}, which is indicated in Figure 1 by a faint vertical line near 10^{-3} mol L^{-1} and 50 mN m^{-1}. Furthermore, *Lunkenheimer et al*. [2003] observed solubility limits in their surface tension measurement of capric acid (C_{10}). Solubility limitations and salting out add to the difficulty of characterizing surface tension, its influence on CCN activity, and the application of models to the process.

Compounds from groups (c) and (d) have direct atmospheric relevance. For example, aromatic dicarboxylic and tricarboxylic acids have been identified in atmospheric samples [*Mochida et al*., 2007]. Organics classified as humic-like substances (HULIS) in ambient samples have been shown to reduce surface tension [*Kiss et al*., 2005; *Taraniuk et al*., 2007]. HULIS is an operationally defined oxygenated oligomer or polycarboxylic acid whose molecular speciation is not fully understood. Compounds fitting this description have been identified in oxidized soot samples [*Decesari et al*., 2002], biomass burning aerosol, photochemically aged secondary organic aerosol [*Baltensperger et al*., 2005], primary emission of marine organic matter, etc. The ambient organic compounds show surface tension reduction similar to that of SDS. Water uptake and CCN activity of aromatic acids and HULIS have been extensively characterized [*Hori et al*., 2003; *Chan and Chan*, 2003; *Brooks et al*., 2004; *Dinar et al*., 2006; *Wex et al*., 2007; *Fors et al*., 2010; *Frosch et al*., 2011; *Kristensen et al*., 2014]. These studies demonstrate that surface active organics take up water and serve as CCN with hygroscopic properties similar in magnitude to nonsurfactant organic compounds. A rigorous analysis explaining the relative role of water activity and surface tension in explaining the CCN activity is not included in these studies, partially due to the absence of detailed molecular information.

The organic carboxylic acids in group (e) weakly reduce surface tension and are identified in ambient samples. Surface tension and CCN activity are well characterized for these compounds [*Shulman et al*., 1996; *Hori et al*., 2003; *Aumann et al*., 2010; *Ekström et al*., 2010]. However, water activity predicts the CCN activity of this class of compounds well [*Petters et al*., 2009a], and the solute concentration in activating drops is likely too small to affect surface tension. The saccharides in group (f) include glucose, which is used in this study as a model nonsurfactant low molecular weight organic substance. As with the compounds in group (e), water activity predicts the CCN activity of saccharides, and surface tension is unlikely to affect droplet activation.

Compounds shown in the foreground of Figure 1 are not found in the atmosphere. However, they are very effective at reducing surface tension, and we propose that they serve as a model to test the CCN activation of strong surfactants. For example, Triton X-100 is nearly as strong a surfactant as the biosurfactants at a similar molar concentration. The estimated concentration of solute at CCN activation for pure Zonyl FS-300, Triton X-100, and SDS are between 10^{-2} and 5×10^{-2} mol L^{-1}, depicted by arrows below the data. Triton X-100 (Polyethylene glycol mono [4-(1,1,3,3-tetramethylbutyl)phenyl] ether)) is a commercially available nonionic surfactant. Zonyl FS-300 is a linear commercial nonionic fluorosurfactant synthesized by a proprietary ethoxylation technique. The surfactant is a mixture with formula $F–(CF_2CF_2)_n–CH_2CH_2O–(CH_2CH_2O)_x–H$, where $3 < n < 8$ and $15 \leq x \leq 25$ [*Cui et al*., 2003; *Ghyzel*, 2013; *Škvarla et al*., 2014]. To our knowledge, CCN activation properties of neither Triton X-100 nor Zonyl FS-300 have been reported in the literature. SDS is included in this study because surface tension is well known [*Rehfeld*, 1967; *Zdziennicka et al*., 2012], and some hygroscopic growth and CCN data are available [*Rood and Williams*, 2001; *Sorjamaa et al*., 2004; *Ruehl et al*., 2010; *Harmon et al*., 2010]. Furthermore, SDS and mixtures of SDS with NaCl have been the experimental basis

21698996, 2016, 4, Downloaded from https://agupubs.onlinelibrary.wiley.com/doi/10.1002/2015JD024090 by University Of California, Wiley Online Library on [01/07/2024]. See the Terms and Conditions (https://onlinelibrary.wiley.com/terms-and-conditions) on Wiley Online Library for rules of use; OA articles are governed by the applicable Creative Commons License

for the validation of Köhler theory that includes surface-to-bulk partitioning [*Li et al*., 1998; *Sorjamaa et al*., 2004; *Prisle et al*., 2008, 2010; *Raatikainen and Laaksonen*, 2011; *Petters and Kreidenweis*, 2013].

Dynamic surface tension measurements of SDS by *Nozière et al*. [2014] show that the minimum value given in Figure 1 is expressed instantaneously but reflects a metastable value that can be further reduced after ~100 s. The effect of dynamic surface tension on CCN activity for the SDS + NaCl system was tested by *Petters et al*. [2013], and results after 6 min were indistinguishable from the control case within measurement uncertainty. Triton X-100 reaches minimum surface tension very quickly (0.02–1 s [*Miller et al*., 1994]), and dynamic surface tension measurements for Zonyl FS-300 were not available.

3. Experimental

The following chemicals and purities were used in this study: deionized water (~18.2 MΩ cm), ammonium sulfate (99.9%, Sigma-Aldrich), sodium chloride (99+ %, Acros), D-(+)- glucose (99.5%, Fisher), sodium dodecyl sulfate (99+ %, Sigma-Aldrich), Triton X-100 (97.5%, Fisher), Zonyl FS-300 (40% solids in water, DuPont), and polystyrene nanospheres (102 ± 3 nm, Thermo Scientific lot #36489). All chemicals were used without further purification.

The measurement setup consists of a spray atomization system that is coupled with a standard size-resolved CCN technique described previously [*Christensen and Petters*, 2012]. Changes to this setup include the atomization procedure and size-scanning strategy and are described below. Aqueous solutions were routed to an atomizer (TSI 3076) by a syringe pump at 10–40 μL min^{-1}. The aerosol stream was then dried by passage through a silica gel diffusion dryer and/or Nafion dryer (PermaPure) and returned to an equilibrium charge distribution using α-radiation (Aerosol Dynamics Inc. casing for ^{210}Po strips) [*Russell et al*., 1996]. Particles were size selected by a differential mobility analyzer (DMA; TSI 308100) operated in scanning mobility particle sizer (SMPS) mode [*Wang and Flagan*, 1990] at room temperature and pressure. Three SMPS voltage ramps were used. Ramp 1 was 2000 to 100 V in 180 s, ramp 2 was 9000 to 1 V in 220 s, and ramp 3 was 10000 to 50 V in 600 s. Diameter bin widths corresponding to 1 Hz data acquisition were 0.8 nm, 2.1 nm, and 0.4 nm, respectively, for diameters between 35 and 90 nm. Ramp choice was guided by optimizing diameter or volume fraction resolution and experiment duration. The sheath to sample flow ratio was 15:1 L min^{-1}/(L min^{-1}). Voltages were converted to diameter by the DMA transfer function [*Knutson and Whitby*, 1975; *Wang and Flagan*, 1990], and the voltage to diameter mapping was verified using polystyrene (PSL) nanospheres. Size spectra were corrected to account for multiply charged particles following the method of *Petters et al*. [2009b]. For PSL tests, DMA size distributions showed a peak that agreed within uncertainty of the manufacturer specifications of the PSL diameters (D = 102 ± 3 nm; Thermo Scientific, lot #36489).

CCN activity was obtained by splitting the size-selected aerosol stream between a condensation particle counter (CPC; TSI 3771) and a CCN counter (CCNC; Droplet Measurement Technologies). A sigmoid activation curve was fit to the ratio of CCN to CPC-inverted size spectra, and the diameter at which 50% of particles activated was recorded as D_d.

Instrument supersaturation was calibrated using the activation diameter of ammonium sulfate (AS) aerosol and the Extended Aerosol Inorganics Model (E-AIM) [*Clegg et al*., 1998; *Wexler and Clegg*, 2002; *Rose et al*., 2008]. Calibration theory and equation are described in section 4.2. Experiments varying supersaturation were calibrated within the same week, and experiments with two-component aerosols were calibrated up to 3 times per experiment. Supersaturation was slightly nonlinear with CCNC column temperature gradient, and no fit line was applied. For six experiments in which both glucose and AS activation diameters were measured, the supersaturation was also calculated using the Margules model of water activity [*Prausnitz et al*., 1999; *Petters et al*., 2009c] for glucose with parameters provided in *Suda and Petters* [2013].

Experiments were performed for pure compounds at different supersaturations by stepping through CCNC nominal column temperature gradients from 6 to 19°C. The proprietary CCN software uses the nominal gradient to set three temperature setpoints along the column [*Christensen and Petters*, 2012], corresponding to water supersaturation ranging from 0.3 to 1.0%. Separate experiments were performed for two-component mixtures varying the volume mixing fraction (including pure compounds) at a constant temperature gradient

21698996, 2016, 4, Downloaded from https://agupubs.onlinelibrary.wiley.com/doi/10.1002/2015JD024090 by University Of California, Wiley Online Library on [01/07/2024]. See the Terms and Conditions (https://onlinelibrary.wiley.com/terms-and-conditions) on Wiley Online Library for rules of use; OA articles are governed by the applicable Creative Commons License

of 8, 10, or 12°C, corresponding to a supersaturation of 0.4, 0.6, or 0.7%. Aqueous two-component solutions were prepared by premixing pure compounds with water at a fixed concentration and then combining these with ±0.5% precision in solute:solute volume fraction. The mixing fractions were atomized in a random order, and the atomizer was rinsed between samples. Pure water was atomized to estimate the contribution of solvent impurities to the atomized sample. Solvent residual volume was ~2% of typical atomized sample volume based on integration over the size distribution.

4. Theory

The relationship between water vapor saturation and the equilibrium diameter of a solution droplet can be described by [*Petters and Kreidenweis*, 2007]

$$S = \frac{D^3 - D_d^3}{D^3 - D_d^3(1-\kappa)} \exp\left(\frac{4\sigma_{s/a} M_w}{RT\rho_w D}\right) \quad (1)$$

where S is the water vapor saturation ratio, D is the solution droplet diameter, D_d is the particle dry diameter, κ is the hygroscopicity parameter, $\sigma_{s/a}$ is the surface tension at the solution/air interface, M_w is the molar mass of water, R is the universal gas constant, T is the temperature, and ρ_w is the density of water. Throughout this work, volume additivity is assumed. The partial molar volumes of solute and water molecules are same as those of pure compounds, which are expected to lead to negligible error [*Kreidenweis et al*., 2005]. A particle is considered activated when the environmental S (i.e., relative humidity (RH)) exceeds a critical saturation ratio defined by $S_c = \max(S)$. Critical supersaturation is defined as $s_c = (S_c - 1) \times 100\%$. A standard κ for comparison between measurements or between models is defined at the reference state of $T = 298.15$ K, surface tension of pure water ($\sigma_0 = 72$ mN m^{-1}), spherical D_d, and fully dissolved solute [*Petters and Kreidenweis*, 2007]. At activation equation (1) at standard state becomes

$$S_c = \max\left[\frac{D^3 - D_d^3}{D^3 - D_d^3(1-\kappa^{\Theta})} \exp\left(\frac{A}{D}\right)\right] \quad (2)$$

where κ^{Θ} is the hygroscopicity parameter at the standard reference state equivalently described as apparent κ (κ_{app}) [*Christensen and Petters*, 2012; *Petters and Kreidenweis*, 2013, and references therein] and $A = 2.1$ nm is the Kelvin diameter of pure water at 298.15 K [*Seinfeld and Pandis*, 2006]. Knowledge of any two of the variables S_c, D_d, and κ^{Θ} allows calculation of the third. The standard state κ^{Θ} serves as a descriptive shorthand for CCN activity derived from experimental data or any of the models described below. Because κ describes intrinsic water uptake and κ^{Θ} is the apparent CCN activity, differences between κ and κ^{Θ} reflect deviations from the assumptions built into equation (2).

4.1. The ZSR Assumption for Ideal Mixing

For mixed particles having two dry components the Zdanovskii-Stokes-Robinson (ZSR) assumption for ideal mixing permits estimation of κ^{Θ}:

$$\kappa^{\Theta} = \varepsilon_1 {\kappa_1}^{\Theta} + (1 - \varepsilon_1){\kappa_2}^{\Theta} \quad (3)$$

where ε is the volume fraction solute in the mixed dry particle and subscripts 1 and 2 refer to components 1 and 2, respectively [*Petters and Kreidenweis*, 2007].

4.2. Incorporating Models of Water Activity

Thermodynamic models such as E-AIM [*Clegg et al*., 1998; *Wexler and Clegg*, 2002] or the Margules model [*Prausnitz et al*., 1999; *Petters et al*., 2009c] describe the activity of water (a_w) as a function of mole fraction water (x_w), providing a necessary reference point for the water uptake of pure compounds. The model-derived $a_w = f(x_w)$ relationship is used to calibrate instrument supersaturation via

$$S = a_w \exp\left(\frac{A}{D_d}\left(1 + \frac{x_w}{1-x_w}\frac{\nu M_w \rho_s}{M_s \rho_w}\right)^{-1/3}\right) \quad (4)$$

where ρ_s is the solute density, M_s is the solute molar mass, ν is the number of dissociable ions of solute, and $S_c = \max(\text{equation (4)})$ varies with only D_d. Instrument supersaturation is found using measured D_d at activation for, e.g., ammonium sulfate and E-AIM or glucose and the Margules model with parameters from *Suda*

21698996, 2016, 4, Downloaded from https://agupubs.onlinelibrary.wiley.com/doi/10.1002/2015JD024090 by University Of California, Wiley Online Library on [01/07/2024]. See the Terms and Conditions (https://onlinelibrary.wiley.com/terms-and-conditions) on Wiley Online Library for rules of use; OA articles are governed by the applicable Creative Commons License

and Petters [2013]. Subsequently, S_c and D_d are used in equation (2) to determine κ^{Θ} by an iterative algorithm. For mixtures in which both $\kappa_1{}^{\Theta}$ and $\kappa_2{}^{\Theta}$ are known, κ^{Θ} is calculated using equation (3).

4.3. Deviations Due To Particle Shape (Model 1)

Deviations between measured and modeled κ^{Θ} may be caused by irregular particle shape. Nonspherical particles have increased drag when passing through the differential mobility analyzer, and thus, the mobility equivalent and volume equivalent diameters differ. The relationship is given by [*Kasper*, 1982; *Hinds*, 1999]

$$D_{me} = \chi D_{ve}\frac{C_c(D_{me})}{C_c(D_{ve})} \qquad C_c(D) = 1 + Kn\left(2.514 + 0.8\exp(-0.55/Kn)\right) \tag{5}$$

where D_{me} is the mobility equivalent diameter, χ is the dynamic shape factor (equal to unity for spheres), D_{ve} is the volume equivalent diameter, C_c is the Cunningham correction factor, λ is the mean free path of air, D is particle diameter, and $Kn = \lambda/D$ is the Knudsen number. Observed D_d corresponds to D_{me}, and thermodynamically modeled D_d corresponds to D_{ve}. If D_{ve} is available from a model prediction via equation (4), χ can be found such that D_{me} = observed D_d.

Ammonium sulfate aerosol may be slightly nonspherical, with a χ that varies with diameter [*Zelenyuk et al.*, 2006] or drying procedure [*Mikhailov et al.*, 2009]. NaCl crystallizes into cubic or nearly cubic particles with an ideal χ of 1.08 in the continuum regime and 1.24 in the free molecular regime [*Hinds*, 1999; *Biskos et al.*, 2006]. Glucose is assumed spherical [*Zelenyuk et al.*, 2006].

For experiments in which both AS and glucose were measured, χ was found such that the shape-corrected AS supersaturation calibration matched the glucose calibration. The retrieved χ's were not applied in the instrument calibration, but results are discussed below. For mixtures containing NaCl, deviations in κ^{Θ} due to χ = 1.02, 1.04, …, 1.16 were modeled as follows. For pure NaCl and pure glucose, D_{ve} was calculated via equation (4) with known instrument supersaturation; D_{me} was calculated via equation (5); and instrument supersaturation and D_{me} were used in equation (2) to determine κ^{Θ} by an iterative algorithm. For pure surfactants the observed κ^{Θ} was used. Finally, equation (3) was used for mixtures. Results are plotted with the observations and discussed below.

4.4. Surfactant Partitioning (Model 2)

Bulk-to-surface partitioning [*Sorjamaa et al.*, 2004; *Raatikainen and Laaksonen*, 2011] is simulated in the κ-framework as described by [*Petters and Kreidenweis*, 2013]

$$\kappa = \varepsilon_{sft}\xi_{sft}\kappa_{sft} + (1 - \varepsilon_{sft})\kappa_{nps} \tag{6a}$$

$$\sigma_{s/a} = \sigma_0 - RT\Gamma_{max}\ln\left(1 + \frac{V_{sft}^{b}}{\alpha_{sft}\beta V}\right) \tag{6b}$$

where "sft" denotes the surfactant, "nps" denotes the nonpartitioning solute, ξ is the fraction of solute residing in the bulk of the droplet (as opposed to the surface), Γ_{max} is the surfactant maximum surface excess, $V_{sft}{}^{b}$ is the volume of dissolved surfactant in the droplet bulk, α is the partial molar volume, β is the surfactant inverse adsorption coefficient, and V is the droplet volume. Equations (6a) and (6b) provide κ and $\sigma_{s/a}$ for use in equation (1), S_c is calculated via S_c = max (equation (1)), and S_c and D_d are used in equation (2) to determine κ^{Θ} by an iterative algorithm.

The values of κ_{sft} and κ_{nps} can be found from hygroscopic growth at high RH. Alternatively, they can be estimated from the compound's molar volume [*Petters et al.*, 2009a]:

$$\kappa_{sft} = \nu\Phi\frac{\alpha_w}{\alpha_{sft}} \tag{7}$$

where Φ is the molal osmotic coefficient (equal to unity for ideal solutions) and α_w is the partial molar volume of water. Volume additivity of bulk α's is assumed in solution such that $\alpha = M/\rho$, where ρ is the bulk density and M is molar mass. For molar volumes $> \sim 500\ \mathrm{cm^3\ mol^{-1}}$ this estimate is modified to account for the dissimilarity in molecular sizes for solute and solvent:

$$\kappa_{sft} = \frac{\alpha_w \times 10^6 + c_1}{\alpha_{sft} \times 10^6} \qquad c_1 = 0.014\left(\alpha_{sft} \times 10^6\right)^{1.14} - 1.4 \tag{8}$$

21698996, 2016, 4, Downloaded from https://agupubs.onlinelibrary.wiley.com/doi/10.1002/2015JD024090 by University Of California, Wiley Online Library on [01/07/2024]. See the Terms and Conditions (https://onlinelibrary.wiley.com/terms-and-conditions) on Wiley Online Library for rules of use; OA articles are governed by the applicable Creative Commons License

Table 1. Three Models of Cloud Condensation Nuclei (CCN) Activity

	Model 1[a] Shape Factor	Model 2[b] Partitioning	Model 3[b] Surface Tension Depression With Prescribed Partitioning
ξ_{sft}	1	equations (9) and (10)	input
$\sigma_{s/a}$	σ_0	equation (6b)	equation (6b)
χ	Input	1	1
D_d	equations (4) and (5)	input	input
κ	ZSR mixing	equation (6a)	equation (6a)
		All Models	
S_c		equation (1)	
κ^{Θ}		equation (2)	

[a] *Kasper* [1982] and *Hinds* [1999].
[b] *Sorjamaa et al.* [2004], *Raatikainen and Laaksonen* [2011], and *Petters and Kreidenweis* [2013].

Equation (8) is an empirical fit for the Flory-Huggins prediction shown in Figure 2 of *Petters et al.* [2009a]. The parameters β and Γ_{max} are found by fitting equation (6b) to bulk surface tension data. Above the critical micelle concentration (cmc), $\sigma_{s/a}$ is equal to its minimum value, σ_{cmc}.

The volume in the bulk is estimated using the analytical formula of *Raatikainen and Laaksonen* [2011]:

$$V_{sft}^{b} = \frac{\alpha_{sft}}{2}\left(g + \sqrt{g^2 + 4\varepsilon_{sft}V_s\beta V/\alpha_{sft}}\right)$$
$$g = \frac{\varepsilon_{sft}V_s}{\alpha_{sft}} - \beta V - \frac{\pi D^2 \Gamma_{max}}{\nu} \quad (9)$$

where V_s is the total volume of solutes. If the solutes share a common counter ion, the cube root solution from equation (8) in *Petters and Kreidenweis* [2013] is used. Finally, the fraction of surfactant residing in the bulk is given by

$$\xi_{sft} = \frac{V_{sft}^{b}}{\varepsilon_{sft}V_s}, \quad (10)$$

and the nonpartitioning solute is assumed to reside completely in the droplet bulk.

4.5. Surface Tension Depression With Prescribed Partitioning (Model 3)

The partitioning model (Model 2) explicitly predicts the fraction of surfactant residing in the droplet bulk (equations (9) and (10)). In contrast, Model 3 uses the same equations as Model 2, but ξ_{sft} is assigned a constant value between 0.01 and 1. Briefly, equation (9) is bypassed; V_{sft}^{b} is determined from equation (10); κ and $\sigma_{s/a}$ are calculated via equations (6a) and (6b); S_c is calculated via $S_c = \max$ (equation (1)), and S_c and D_d are used in equation (2) to determine κ^{Θ} as before. Importantly, note that for $\xi_{sft} = 1.0$, Model 3 is equivalent to the standard state except it includes surface tension depression (without surfactant partitioning) and is conceptually equivalent to the models used by *Ekström et al.* [2009, 2010], *Padró et al.* [2010], *Giordano et al.* [2013], and *Nozière et al.* [2014]. This model is implemented for comparison due to its popularity. Models 1–3 are summarized in Table 1.

5. Results

5.1. Chemical Properties

Table 2 summarizes the physicochemical properties of the compounds used in this study. The κ_{sft} values are obtained from *Ruehl et al.* [2010] for SDS and by equation (8) for Triton X-100 and Zonyl FS-300. Table 3 shows the results of fitting equation (6b) to bulk surface tension data for SDS, Triton X-100, and Zonyl FS-300 from the literature, and Figure 1 displays the fitted curves. Two measurement sets for SDS are in very good agreement. Due to the paucity of data for Zonyl FS-300, four different fits span the range of possible molar masses and Γ_{max} values emulating either the similar compound Zonyl FSN-100 or Triton X-100.

5.2. CCN Activity for Pure Compounds at Different Supersaturations

Figures 2, 3 summarize CCN experiments for pure compounds at different supersaturations (data are available in the supporting information). These experiments were performed over a period of ~2 weeks following voltage ramp 3

21698996, 2016, 4, Downloaded from https://agupubs.onlinelibrary.wiley.com/doi/10.1002/2015JD024090 by University Of California, Wiley Online Library on [01/07/2024]. See the Terms and Conditions (https://onlinelibrary.wiley.com/terms-and-conditions) on Wiley Online Library for rules of use; OA articles are governed by the applicable Creative Commons License

Table 2. Physicochemical Properties

	α ($m^3\ mol^{-1}$)	ν (−)	κ_{nps} (−)
glucose[a,b]	1.1534×10^{-4}	1	0.162
ammonium sulfate[c]	7.4698×10^{-5}	3	0.63
sodium chloride[c]	2.7056×10^{-5}	2	1.28
			κ_{sft} (−)
sodium dodecyl sulfate[d,e]	2.4522×10^{-4}	2	0.134
Triton X-100[f,h]	6.0623×10^{-4}	1	6.18×10^{-2}
Zonyl FS-300[g,h]	9.32×10^{-4} to 1.79×10^{-3}	1	4.93×10^{-2} to 5.43×10^{-2}

[a] ρ and M_s from *Haynes* [2015].
[b] κ_{nps} from Margules model [*Prausnitz et al*., 1999; *Petters et al*., 2009a] using parameters from *Suda and Petters* [2013].
[c] κ_{nps} from E-AIM [*Clegg et al*., 1998; *Wexler and Clegg*, 2002].
[d] ρ from *Sorjamaa et al*. [2004] and M_s from *Haynes* [2015].
[e] κ_{sft} from hygroscopic growth at high RH; [*Ruehl et al*. 2010].
[f] ρ, M_s, and ν from Acros Organics product specifications.
[g] Ranges based on formulas in *Cui et al*. [2003], formula for Zonyl FSN-100 in *Škvarla et al*. [2014], formulas given in *Ghyzel* [2013], and DuPont technical data sheet.
[h] κ_{sft} is calculated from equation (8) and using ρ_w recommended by *Wagner and Pruß* [2002].

with a κ^e bin width of 2% (calculated from diameter bin width as $(\kappa^e(D_{bin\ i+1})-\kappa^e(D_{bin\ i}))/\kappa^e(D_{bin\ i}) \times 100\%$). Summary statistics for these data are given in Table 4.

Results for pure nonsurfactants are shown in Figure 2. These experiments include two repeats for AS and one repeat for glucose. Ammonium sulfate κ^e increased with diameter, and the values agree with E-AIM because they were used to define the instrument supersaturation. The average κ^e drifted ±1.2% over three experiments. NaCl κ^e also increased with diameter but fell well below the value predicted by E-AIM. Shape factors for NaCl forcing the data to agree with E-AIM (Model 1) decreased from 1.15 to 1.11 as diameter increased from 24 to 53 nm. The observed absolute values and diameter trends for shape factors are consistent with literature values. *Wang et al*. [2010] report $\chi = 1.06$ to 1.26 for 35 to 40 nm particles. *Zelenyuk et al*. [2006] report χ increasing from 1.06 to 1.17 for 200 to 800 nm particles. Glucose κ^e decreased slightly with diameter and was 10% higher than predicted from the Margules water activity model, which is based on hygroscopic growth factor data and bulk water activity measurements [*Suda and Petters*, 2013]. This correspondence between measured hygroscopic growth factors and bulk water activity in the subsaturated and supersaturated regime indicates that potentially glassy dry glucose particles are not kinetically limited. The second glucose experiments κ^e drifted relative to the first by 3.5%.

Experiments with pure surfactants at different supersaturations are summarized in Figure 3. The relative spread in Triton X-100 κ^e was approximately 1 order of magnitude larger than those of the other compounds, including the nonsurfactants. Weak trends in κ^e with supersaturation were observed for SDS and Triton X-100: SDS κ^e decreased by 8% between 46 and 108 nm and Triton X-100 κ^e decreased by 25% between 52 and 131 nm. No trend was observed for Zonyl FS-300. Constant κ_{sft}'s corresponding to hygroscopic

Table 3. Properties of Surfactants[a]

	β ($mol\ m^{-3}$)	Γ_{max} ($mol\ m^{-2}$)	σ_{cmc} ($mN\ m^{-1}$)
sodium dodecyl sulfate[b]	2.056	8.7×10^{-6}	38.4
Triton X-100[b]	1.0×10^{-3}	2.8×10^{-6}	37.7
Zonyl FS-300[c,d]	7.2×10^{-2}	3.5×10^{-6}	23
Zonyl FS-300[c,e]	2.1×10^{-2}	2.8×10^{-6}	23
Zonyl FS-300[c,f]	3.6×10^{-2}	3.5×10^{-6}	23
Zonyl FS-300[c,g]	1.0×10^{-2}	2.8×10^{-6}	23

[a] Properties were found by fitting equation (6b) to literature data.
[b] *Zdziennicka et al*. [2012].
[c] DuPont technical data sheet; *Cui et al*. [2003]; *Ghyzel* [2013]; *Škvarla et al*. [2014]; and molar volume (α) estimates are in Table 2.
[d] Γ_{max} held fixed to Zonyl FSN-100 value [*Škvarla et al*., 2014]; upper estimate of α.
[e] Γ_{max} held fixed to Triton X-100 value; upper estimate of α.
[f] Γ_{max} held fixed to Zonyl FSN-100 value; lower estimate of α.
[g] Γ_{max} held fixed to Triton X-100 value; lower estimate of α.

21698996, 2016, 4, Downloaded from https://agupubs.onlinelibrary.wiley.com/doi/10.1002/2015JD024090 by University Of California, Wiley Online Library on [01/07/2024]. See the Terms and Conditions (https://onlinelibrary.wiley.com/terms-and-conditions) on Wiley Online Library for rules of use; OA articles are governed by the applicable Creative Commons License

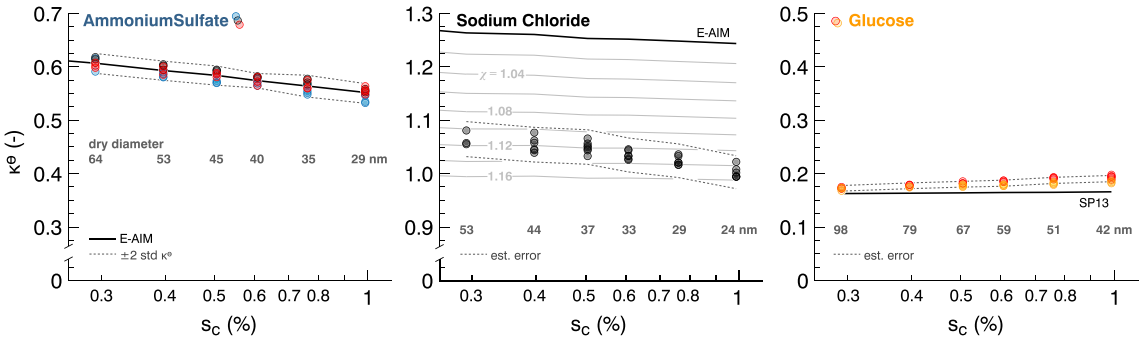

Figure 2. Hygroscopicity parameter κ^{Θ} for pure nonsurfactant solutes at different supersaturations. Colors represent repeats on separate days. Black lines correspond to equation (4) using E-AIM or the Margules model with parameters from *Suda and Petters* [2013] ("SP13"). Solid grey lines in the second panel show Model 1 κ^{Θ} for different values of χ. Dotted grey lines show estimated error based on the calibration ±2 standard deviation κ^{Θ} (= ±3.083% κ^{Θ}) in the first panel. The average measured D_d's are indicated below the data.

growth (given in Table 2) were ~1% higher, 25% lower, and 50% lower than measured κ^{Θ}'s for SDS, Triton X-100, and Zonyl FS-300, respectively; in the same order, Model 2 predictions were ~10% higher, 40% lower, and 80% lower than the measurements. Model 3 predictions with $\xi_{sft} = 1$ (surface tension depression without partitioning) were 400+ % higher than the measurements. A sharp decrease in the Model 3 with $\xi_{sft} = 1$ prediction for SDS arose from the discontinuity in surface tension at the critical micelle concentration. SDS and Triton X-100 measurements are circumscribed by the $\xi_{sft} = 0.1$ and 0.2 isolines. Zonyl FS-300 κ^{Θ}'s crossed ξ_{sft} isolines from 0.05 to nearly 0.1.

5.3. CCN Activity for Mixtures at Different Mixing Ratios

Figures 4–8 summarize CCN experiments at different mixing ratios (data are available in the supporting information). These experiments were performed over a period of ~3 years and implicitly include measurements for pure compounds. Unlike the experiments presented above, all three voltage ramps were used, and the experiments were performed at constant supersaturation. Summary statistics for pure compounds at the endpoints of mixing experiments are given in Table 4. These average κ^{Θ}'s agree within ±10% of those

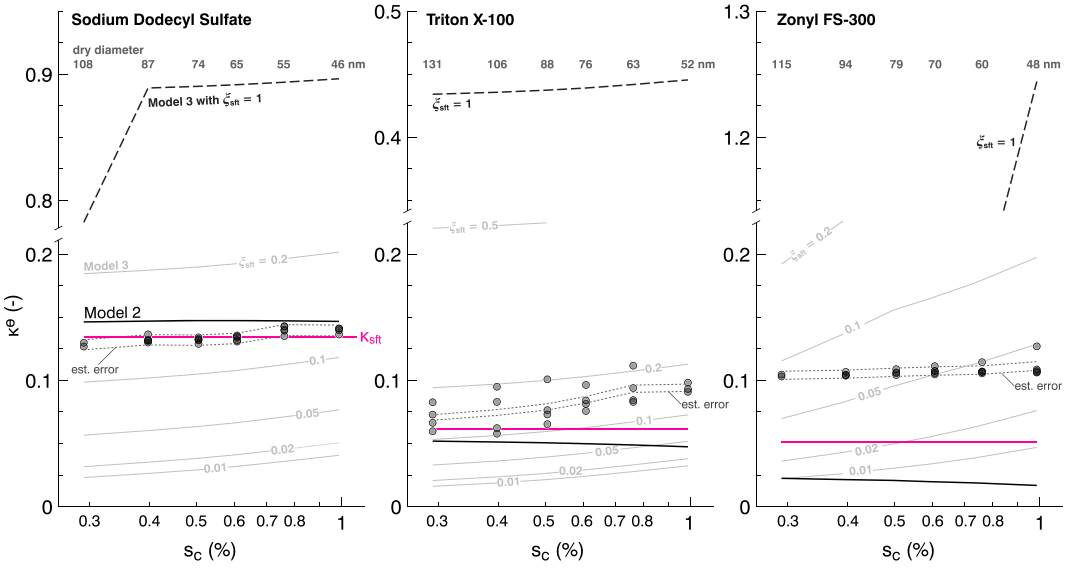

Figure 3. Hygroscopicity parameter κ^{Θ} for pure surfactants at different supersaturations. Note the scale break between lower and higher κ^{Θ}. Lines correspond to κ_{sft} from Table 2 (pink), Model 2 (solid black), Model 3 with $\xi_{sft} = 0.01$ to 0.50 (grey with printed ξ_{sft}), and with $\xi_{sft} = 1$ (dashed black). Models of Zonyl correspond to averages over four parameter sets (Table 3). Dotted grey lines show estimated error based on the calibration (Figure 2). Average measured D_d's are indicated above the data.

21698996, 2016, 4, Downloaded from https://agupubs.onlinelibrary.wiley.com/doi/10.1002/2015JD024090 by University Of California, Wiley Online Library on [01/07/2024]. See the Terms and Conditions (https://onlinelibrary.wiley.com/terms-and-conditions) on Wiley Online Library for rules of use; OA articles are governed by the applicable Creative Commons License

Table 4. Measured κ^{Θ} for Pure Compounds[a]

	At Different Supersaturations			Endpoints of Mixing Experiments			
	avg κ^{Θ} (−)	SD κ^{Θ} (%)	n (−)	avg κ^{Θ} (−)	SD κ^{Θ} (%)	n (−)	±2 SD κ^{Θ} (−)
glucose	0.181	2.1	47	0.168	5.3	16	0.151–0.186
ammonium sulfate	0.579	1.5	64	0.581	4.1	41	0.534–0.629
sodium chloride	1.038	1.1	34	1.130	5.9	15	0.997–1.26
sodium dodecyl sulfate	0.135	1.7	26	0.136	21	14	0.0783–0.194
Triton X-100	0.082	14.2	24	0.0907	21	11	0.0518–0.130
Zonyl FS-300	0.107	1.8	24	0.102	11	9	0.0789–0.125

[a] n is the sample size; the standard deviation in κ^{Θ} for pure compounds at different supersaturations is the average of standard deviations calculated at each supersaturation.

retrieved for pure component experiments at different supersaturations. The data are discussed in the following order: glucose with AS; glucose with NaCl; SDS with glucose, AS, or NaCl; Triton X-100 with glucose, AS, or NaCl; and Zonyl FS-300 with glucose, AS, or NaCl. Mixing of glucose with inorganics is included to explore repeatability and examine potential effects due to solute-solute interactions and nonspherical particle shape.

Six independent experiments mixing glucose with AS are shown in Figure 4. Experiments were calibrated by AS and followed voltage ramp 1 or 2 corresponding to κ^{Θ} bin widths of 2% or 6–11%. Measured D_d's and supersaturations for pure AS and pure glucose endpoints are presented in Table 5. Expected κ^{Θ} from water activity (E-AIM and Margules models) varied by ~3% and 1% relative to the mean for AS and glucose, respectively. The difference in κ^{Θ} between AS and glucose was consistent over all the experiments. The supersaturation calculated from glucose measurements was consistently close to the AS calibration (best fit $s_{c,gluc} = 0.914 \times s_{c,AS} + 0.040$, $n = 6$, $R^2 = 0.991$; $R^2 = 0.982$ relative to 1:1 line). Ammonium sulfate χ's calculated via Model 1 such that the calibrations agreed are summarized in Table 5. Some values are $\chi < 1$. No correlation with particle size was observed. This indicates that shape factors for AS and glucose were similar and likely close to spherical in those experiments. Observed variability in χ is due to random measurement error. Based on this result, all of the experiments were calibrated on AS without further shape correction. Figure 4 shows that the observed κ^{Θ} approximately follows the linear ZSR mixing rule. For $0.20 < \varepsilon_{AS} < 0.80$, observed κ^{Θ} is 3–13% lower than the ZSR estimate, which may be indicative of solute-solute interactions.

Experiments mixing glucose with NaCl are shown in Figure 5. Voltage ramp 2 was used corresponding to a κ^{Θ} bin width of 6–11%. The trend in κ^{Θ} is linear but falls significantly below the ZSR estimate. For mixing fractions above $\varepsilon_{NaCl} = 0.20$ the measurements coincide with $\chi = 1.05$ to 1.13 with an average of 1.09. The χ retrieved using Model 1 was nearly constant above $\varepsilon_{NaCl} = 0.20$. These values are consistent with those reported in Figure 2 and suggest that the mixed particles are nonspherical. However, solute-solute interactions likely contributed to deviations from the ZSR estimate, especially at ε_{NaCl} lower than ~0.7. Figure 5 also illustrates the random measurement sequence of solutions, which was adopted for all mixing experiments. The results demonstrate that there is no carryover between atomized solutions of different compositions.

Experiments mixing SDS with glucose, AS, or NaCl are shown in Figure 6. The κ^{Θ}'s correspond to measured D_d ranges of 75–87 nm at an instrument supersaturation of 0.42% (SDS + glucose), 41–68 nm at 0.59% (SDS + AS), and 38–81 nm at 0.46% (SDS + NaCl). Voltage ramps corresponded to κ^{Θ} bin widths of 4–8% (SDS + glucose) and 2–4% (all others). The CCN activity of glucose mixtures fell below the ZSR mixing line at high SDS fraction and above ZSR mixing at $\varepsilon_{glucose} \geq 0.60$. Data falling outside the envelope ±2 standard deviation κ^{Θ} predicted from the ZSR model (hereafter denoted ZSR envelope; see Table 4 for endpoints) will be highlighted in the following. The CCN activity of glucose mixtures was entirely within the ZSR envelope. The CCN activity of AS mixtures fell above the ZSR mixing line at $\varepsilon_{AS} \geq 0.50$, and below the ZSR mixing line at high SDS fraction, falling outside the ZSR envelope at ε_{AS} ~0.20. The CCN activity of NaCl mixture κ^{Θ}'s fell below the ZSR envelope at ε_{NaCl} ~0.10 and ε_{NaCl} ~0.95–1.00. The NaCl mixture κ^{Θ}'s coincided with $\chi =$ ~1.08 at $\varepsilon_{NaCl} \geq 0.80$. Scatter in κ^{Θ} within individual experiments was ±4%, lower than the scatter given in Table 4 for pure glucose or SDS over all mixing experiments. At high SDS fraction Model 2 predicted $\kappa^{\Theta} > \kappa_{sft}$ due to the effect of surface tension on s_c in equation (1), except in the case SDS + NaCl, where the common counter ion reduced the bulk concentration of SDS entering equation (6a).

21698996, 2016, 4, Downloaded from https://agupubs.onlinelibrary.wiley.com/doi/10.1002/2015JD024090 by University Of California, Wiley Online Library on [01/07/2024]. See the Terms and Conditions (https://onlinelibrary.wiley.com/terms-and-conditions) on Wiley Online Library for rules of use; OA articles are governed by the applicable Creative Commons License

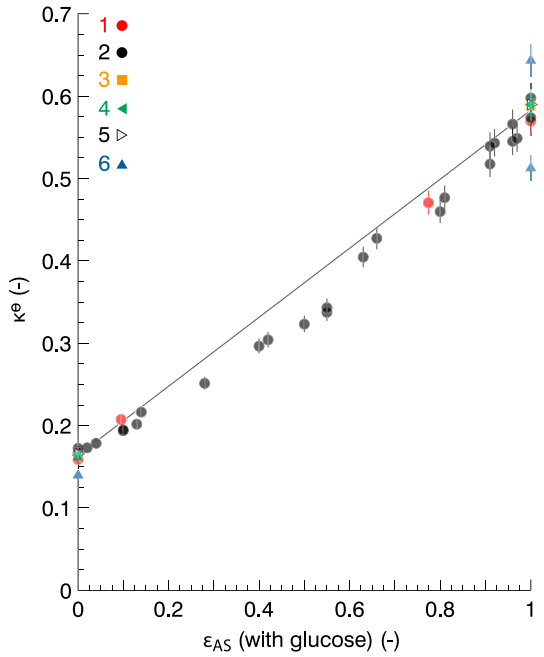

Figure 4. Hygroscopicity parameter κ^{Θ} for glucose mixed with ammonium sulfate (AS), where ε_{AS} is the volume fraction AS in the dry particle. The black line corresponds to the ZSR estimate based on the ideal κ^{Θ} for glucose (Margules model) and AS (E-AIM). Vertical bars indicate estimated error as in Figure 2. Numbers indicate an experiment number and can be matched to the data in Table 5.

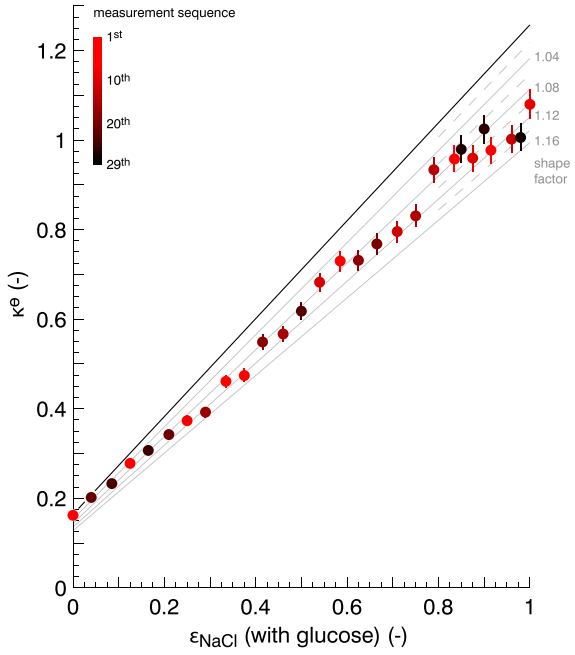

Figure 5. Hygroscopicity parameter κ^{Θ} for glucose mixed with sodium chloride (NaCl), where ε_{NaCl} is the volume fraction NaCl in the dry particle. Colors indicate the random order in which the mixing fractions were tested. The black line corresponds to the ZSR estimate based on the ideal κ^{Θ} for glucose (Margules model) and NaCl (E-AIM). Vertical bars indicate estimated eror as in Figure 2. Grey lines show Model 1 κ^{Θ} for different values of χ.

Experiments' mixing Triton X-100 with glucose, AS, or NaCl are shown in Figure 7. The κ^{Θ}s correspond to measured D_d ranges of 77–98 nm at an instrument supersaturation of 0.42% (Triton + glucose; red and black symbols), 49–107 nm at 0.43% (Triton + AS; red and black), 53–99 nm at 0.39% (Triton + AS; blue, green, and orange), 39–107 nm at 0.43% (Triton + NaCl; red and black), and 43–97 nm at 0.40% (Triton + NaCl; blue and green). Voltage ramps corresponded to κ^{Θ} bin width of 8–10% (red and black) or 2% (blue, green, and orange). The CCN activity near equal mixing fraction fell 20% below the ZSR line for glucose mixtures and 40% below the line for AS and NaCl mixtures. For AS and NaCl many measurements fell in the space 0–40% below ZSR mixing. Measured $\kappa^{\Theta\prime}$s fell outside the ZSR envelope near equal mixing fractions. The NaCl mixture $\kappa^{\Theta\prime}$s coincided with $\chi = 1.02$–1.08 at $\varepsilon_{NaCl} \geq 0.90$. Scatter in κ^{Θ} within individual experiments was ~ ±5% but closer to ±10–20% when considering scatter between repeated experiments. Model 2 predicted linear κ^{Θ} mixing at low Triton fraction ($\varepsilon_{glucose} > \sim 0.40$, $\varepsilon_{AS} > \sim 0.10$, and $\varepsilon_{NaCl} > \sim 0.05$) with an upward curve in κ^{Θ} at high Triton fraction. The model was insensitive to D_d except at high Triton fraction. For pure Triton the predicted κ^{Θ} was 0.051, 43% lower than the average measurement.

Experiments mixing Zonyl FS-300 with glucose, AS, or NaCl are shown in Figure 8. The $\kappa^{\Theta\prime}$s correspond to measured D_d ranges of 62–72 nm at an instrument supersaturation of 0.59% (Zonyl + glucose), 51–93 nm at 0.42% (Zonyl + AS), and 39–91 nm at 0.42% (Zonyl + NaCl). Voltage ramps corresponded to κ^{Θ} bin widths of 2–4% (Zonyl + glucose) or 6–11% (all others). The CCN activity of glucose mixtures was linear as a function of $\varepsilon_{glucose}$ and fell at most 15% below the ZSR mixing line as $\varepsilon_{glucose}$ approached unity, leaving the ZSR envelope at $\varepsilon_{glucose} \geq 0.60$. The CCN activity of AS mixtures fell below the ZSR line by up to 40% near equal

21698996, 2016, 4, Downloaded from https://agupubs.onlinelibrary.wiley.com/doi/10.1002/2015JD024090 by University Of California, Wiley Online Library on [01/07/2024]. See the Terms and Conditions (https://onlinelibrary.wiley.com/terms-and-conditions) on Wiley Online Library for rules of use; OA articles are governed by the applicable Creative Commons License

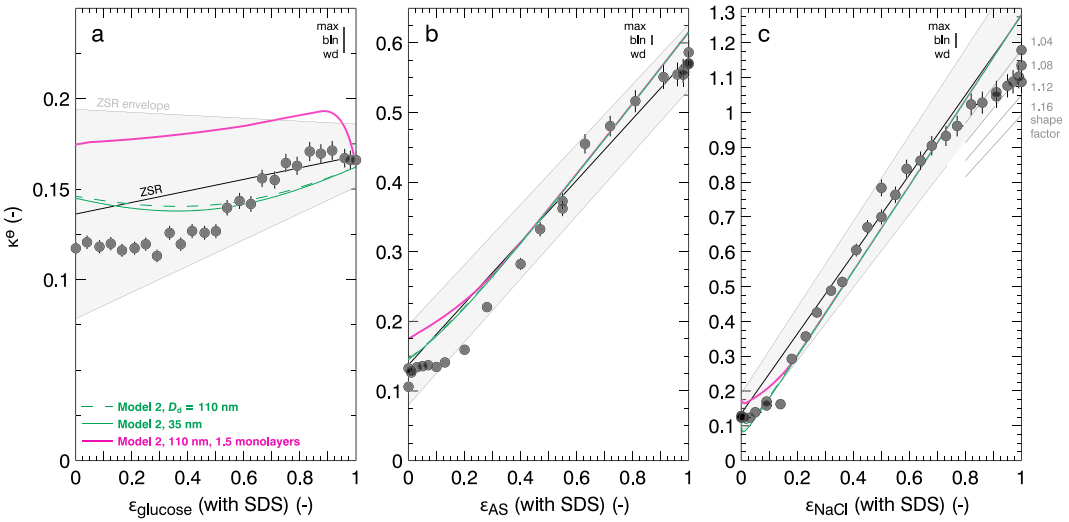

Figure 6. Hygroscopicity parameter κ^{Θ} for sodium dodecyl sulfate (SDS) mixed with (a) glucose, (b) ammonium sulfate (AS), and (c) sodium chloride (NaCl), where ε_X is the volume fraction X in the dry particle. Black lines correspond to ZSR mixing based on the average κ^{Θ} (Table 4) or the ideal E-AIM κ^{Θ} (NaCl), and shaded areas correspond to the ZSR envelope of ±2 standard deviation κ^{Θ}. Green lines show Model 2 predictions for 110 nm and 35 nm particles. Magenta lines show Model 2 predictions for 110 nm particles with a maximum surface excess of 1.5 monolayers (see section 6). Vertical bars indicate estimated error as in Figure 2. Grey lines in Figure 6c show Model 1 κ^{Θ} for different values of χ.

mixing fractions, similar to the Triton mixtures described above. The measurements fell outside the ZSR envelope where $0.10 \le \varepsilon_{AS} \le 0.80$ but then increase by ~35% between $\varepsilon_{AS} = 0.80$ and 0.90. The CCN activity of NaCl mixtures is within ±20% of the ZSR mixing line, falling often above the line where $\varepsilon_{NaCl} \ge 0.40$. Measurements were above the ZSR envelope in the range $0.30 \le \varepsilon_{NaCl} \le 0.70$ and below the envelope at $\varepsilon_{NaCl} \sim 0.20$. Measured κ^{Θ} coincided with $\chi = 1.00$–1.04 at $\varepsilon_{NaCl} \ge 0.95$. These were the only NaCl measurements where χ was $<$ ~1.08. Model 2 predicted linear κ^{Θ} mixing at low Zonyl fraction ($\varepsilon_{glucose} >$ ~0.20, $\varepsilon_{AS} >$ ~ 0.05, and $\varepsilon_{NaCl} >$ ~0.025) with an upward curve at high Zonyl fraction, which is similar to the Triton X-100 prediction. The model was also insensitive to D_d except at high Zonyl fraction. Model 2 predicted a κ^{Θ} of 5×10^{-3}–0.0323 for pure Zonyl, 68–95% lower than the measurement.

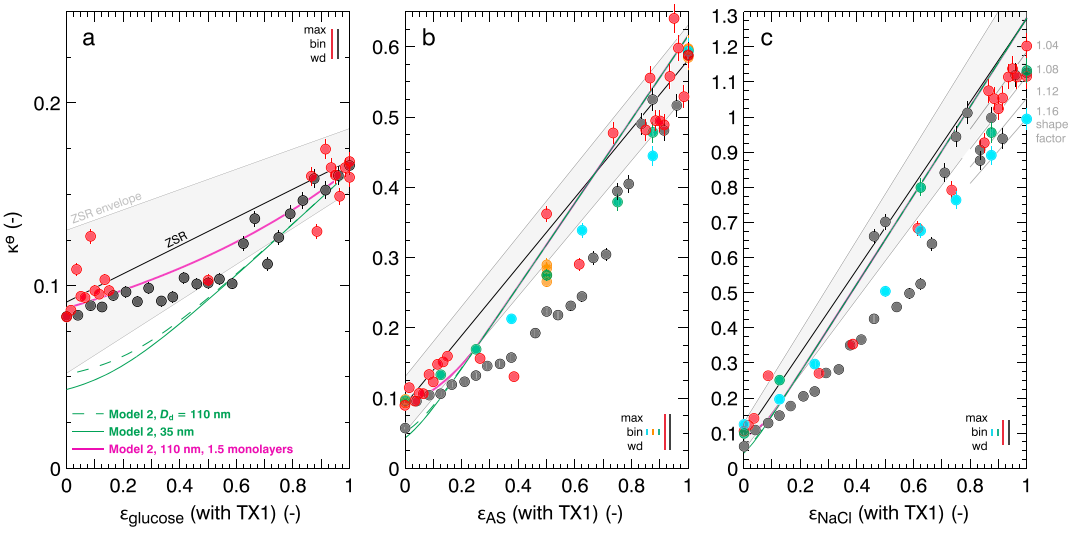

Figure 7. Same as Figure 6 but for Triton X-100 (TX1) mixed with (a) glucose, (b) ammonium sulfate (AS), and (c) sodium chloride (NaCl). Different symbol colors correspond to repeat experiments.

21698996, 2016, 4, Downloaded from https://agupubs.onlinelibrary.wiley.com/doi/10.1002/2015JD024090 by University Of California, Wiley Online Library on [01/07/2024]. See the Terms and Conditions (https://onlinelibrary.wiley.com/terms-and-conditions) on Wiley Online Library for rules of use; OA articles are governed by the applicable Creative Commons License

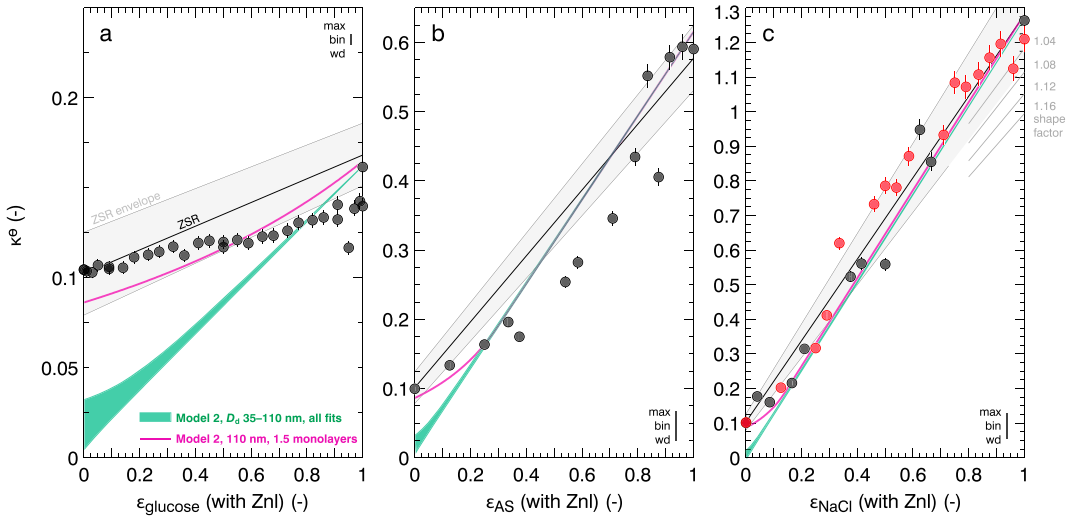

Figure 8. Same as Figure 6 but for Zonyl FS-300 (ZnI) mixed with (a) glucose, (b) ammonium sulfate (AS), and (c) sodium chloride (NaCl). Green shaded regions show the range in Model 2 predictions for 110–35 nm particles over all ZnI properties listed in Tables 2 and 3. The red symbols in Figure 8c are a repeat experiment.

6. Discussion

The model without accounting for bulk-to-surface partitioning (Model 3, $\xi_{sft} = 1$, cf. Figure 3) predicted κ^e several hundred percent higher than the measurements. For pure SDS, κ^e was within 2% of κ, implying that CCN activity was not enhanced relative to intrinsic water uptake. In fact, the SDS κ^e was 10% lower than the molar volume estimate of $\kappa_{sft} = 0.147$ from equation (7). By contrast, the Triton X-100 and Zonyl FS-300 κ^e measurements were higher than predicted by κ_{sft} from equation (8) by 30% and 50%, respectively. This enhancement for pure compounds could be due to surface tension reduction. The partitioning model (Model 2) did not enhance the predicted κ^e relative to κ_{sft} but lowered it further. *Irwin et al.* [2010] made a similar observation. The predicted strong depletion of the bulk, indicated by the low ξ_{sft} values in Figure 3, implies up to 15 monolayers of surfactant in the surface phase. However, a maximum adsorption density is implied by adsorption theory and approximated by Γ_{max}. A simple adjustment limiting the surface phase to 1.5 monolayers increased the predicted κ^e to coincide with the measurements for Zonyl and Triton X-100. Monolayer thickness was estimated using the molar cross-sectional area ($1/\Gamma_{max}$), equivalent to the area extruded by 1 mol at maximum packing density. The molar cross-sectional area was used to obtain a proxy molecular diameter $D = (4/(\pi\Gamma_{max} N_A))^{1/2}$, where N_A is Avogadro's number, which was taken to be the width of one monolayer. The volume of surfactant in the surface phase was constrained by this layer's volume. Figures 6–8 show that limiting the number of surface monolayers to 1.5 for mixtures generally improves the predictions, except for SDS + glucose or AS (Figures 6a and 6b). In these cases, the prediction is worsened as

Table 5. Summary of Pure Ammonium Sulfate and Glucose Measurements[a]

		Ammonium Sulfate			Glucose					
	dT (°C)	D_d (nm)	m (–)	s_c (%)	$D_{d,gluc}$ (nm)	m (–)	$s_{c,gluc}$ (%)	χ (–)	κ_{gluc}^e (–)	κ_{AS}^e (–)
1	12	37	7	0.69	57	7	0.67	0.980	0.159	0.570
2	8	47	6	0.47	72	4	0.48	1.022	0.167	0.598
		48	9		70	5			0.173	0.574
3	8	49	2	0.44	76	4	0.44	0.996	0.162	0.588
4	8	51	3	0.42	77	3	0.43	1.013	0.169	0.590
5	8	51	3	0.42	77	3	0.43	1.005	0.166	0.590
6	10	43	3	0.59	63	5	0.56	0.954	0.162	0.643
		40	4		66	3			0.140	0.513

[a] dT is the CCN instrument temperature gradient, m is the number of repeated scans associated with the reported κ^e, χ is the ammonium sulfate dynamic shape factor forcing the two calibrations to agree, and κ_{gluc}^e and κ_{AS}^e are the measured κ^e's for glucose and ammonium sulfate, shown in Figure 4.

21698996, 2016, 4, Downloaded from https://agupubs.onlinelibrary.wiley.com/doi/10.1002/2015JD024090 by University Of California, Wiley Online Library on [01/07/2024]. See the Terms and Conditions (https://onlinelibrary.wiley.com/terms-and-conditions) on Wiley Online Library for rules of use; OA articles are governed by the applicable Creative Commons License

21698996, 2016, 4, Downloaded from https://agupubs.onlinelibrary.wiley.com/doi/10.1002/2015JD024090 by University Of California, Wiley Online Library on [01/07/2024]. See the Terms and Conditions (https://onlinelibrary.wiley.com/terms-and-conditions) on Wiley Online Library for rules of use; OA articles are governed by the applicable Creative Commons License

limiting surface adsorption increases the predicted κ^{Θ}. Perfect agreement with data is not achieved due to effects discussed in the next paragraphs. Nevertheless, the overall improved prediction due to imposing a reasonable physical constraint supports the validity of partitioning theory. The sensitivity of the prediction to the constraint will limit high-accuracy predictions from surface tension data since it is not a priori clear how many monolayers of adsorption should be permitted. Experimental and modeling techniques that probe the physical thickness of the surface layer in growing submicron droplets [*Ruehl and Wilson*, 2014; *Werner et al*., 2014] will be needed to inform the existing framework.

In general, all of the models shown in Figures 6–8 only imperfectly capture the shape of the κ^{Θ} versus volume fraction relationship. One reason for this is the high sensitivity of κ^{Θ} to changes in diameter, supersaturation, and composition. Factors such as solute-solute interactions, solute-water interactions, solution impurities, particle shape, deviation from volume additivity, and fractionation effects in the atomization step (imperfect mixing) play a role. Some of these factors are associated with the limit of observability using current instrumentation and experimental design. For example, perfectly spherical particles with exactly known composition could not be prepared. Other factors are associated with necessary model assumptions. For example, activity coefficients for mixed particles are unknown. We now discuss several of these factors in greater detail.

6.1. Solute-Solute and Solute-Water Interactions

Model 2 worked well for the mixture of SDS + NaCl but did not anticipate the functional form of κ^{Θ} versus mixing fraction for other systems, especially at high surfactant fraction. ZSR mixing did not describe the results either. A dip in the center of four of the mixing plots (Triton + anything and Zonyl + AS) appears to be unrelated to surface tension, based on the fact that the largest deviation is near equal mixing fractions and not at high surfactant fraction. The deviation could instead be due to solute-solute and solute-water interactions, e.g., variable activity coefficients for different mixing ratios of the solutes and different dilutions with water. Strong solute-solute interactions could also lead to deviation from volume additivity, although this effect is expected to be minor at the point of droplet activation [*Kreidenweis et al*., 2005]. The surfactants and salts tested are weakly functionalized and perhaps should not be expected to behave ideally in mixtures [*Suda et al*., 2014]. A very similar dip was observed by *Kristensen et al*. [2014] for Nordic Aquatic Fulvic Acid mixed with NaCl. The observations are also consistent with observations for multicomponent organic mixtures that show that the combined particle is usually slightly less hygroscopic than one would expect from ZSR [*Suda et al*., 2012].

One unresolved question is how solubility and critical micelle concentration should be treated. If micelles are formed, the entropy of mixing is reduced, and water activity likely deviates from Raoult's law or the Flory-Huggins predictions. This may be accounted for to first order in the parameterized κ taken from measurements at RH > 99% [*Ruehl et al*., 2010] that is used to initialize the model. At that RH, the model predicts composition that thermodynamically favors micelle formation. The parameterized approach, however, does not treat the true multiphase equilibrium consisting of a potentially present solid, aqueous micelle, organic rich aqueous, organic poor aqueous, and surface phases. Fully accounting for the interaction of solutes and water in the droplet is beyond the scope of this work but may be necessary to better capture the κ^{Θ} versus volume fraction relationship.

6.2. Solution Impurities

Model 2 makes a distinctive prediction of strongly nonlinear behavior for mixtures of SDS + NaCl near $\varepsilon_{NaCl} = 0.05$ (Figure 6c). This effect is due to interactions of the common counter ion Na^+ in the solutes. The measurement agrees reasonably well with the prediction, but impurities in the chemicals used and in the deionized water introduce error. Our test atomizing pure water suggested that impurities contribute ~2% to the mixed aerosols, enough to blur resolution in ε. Note that a similar shape was observed for SDS mixed with AS (at $\varepsilon_{AS} = 0$–0.1), which the theory did not predict (Figure 6b). The similar salting out effect has also been difficult to confirm in the past [*Frosch et al*., 2011; *Prisle et al*., 2012], and counter ion interaction is inconclusive at the present measurement resolution.

6.3. Particle Shape for Mixtures Containing NaCl

Based on the consistent offset of κ^{Θ} from the ZSR or Model 2 prediction in Figures 5–7, it seems that particles mixed with NaCl were nonspherical at high ε_{NaCl}. This is a reasonable conclusion for pure NaCl and above a

21698996, 2016, 4, Downloaded from https://agupubs.onlinelibrary.wiley.com/doi/10.1002/2015JD024090 by University Of California, Wiley Online Library on [01/07/2024]. See the Terms and Conditions (https://onlinelibrary.wiley.com/terms-and-conditions) on Wiley Online Library for rules of use; OA articles are governed by the applicable Creative Commons License

certain ε_{NaCl}; however, it is not clear at what fraction other factors contribute to non-ZSR mixing. The glucose + NaCl seems to maintain a constant $\chi \sim 1.08$ above $\varepsilon_{NaCl} \sim 0.20$, but this is just as likely to be a manifestation of a depression in CCN activity near $\varepsilon_{NaCl} = 0.50$ superimposed over the effect of nonspherical shapes. Note that the Zonyl + NaCl mixture shows $\chi \sim 1$ at high NaCl mixing fraction, contrary the other mixtures. The potential role of particle shape in measured D_d and calibrated supersaturation combined with the influence of particle size, activity coefficients, and surface partitioning on κ^{Θ} poses a fundamental limit on how well theory predictions can be constrained with these types of measurements.

6.4. Fractionation Effects

Scatter in the measurements with Triton X-100 was much higher than for other compounds. Some experiments in Figures 7b and 7c follow the ZSR mixing line, and others strongly deviate. Notably, this dichotomy seems to appear on experiments conducted the same day and occurred in random order. Suspecting possible instrument malfunction or too fast of a scan rate, we performed a large number of repeats using different voltage ramps, different random sample measurement order, and fresh stock solutions. None of these conclusively reduced the scatter. One possible explanation is that the spray atomizer alters the surfactant fraction in the mixture relative to the stock solution and that this effect is unsteady over time. *MacMillan et al*. [2012] observed fractionation effects with electrospray atomization of SDS mixtures. However, the pure compound measurements in Figure 3 were all collected at high resolution under the same settings, and pure Triton has an order of magnitude higher scatter than all other compounds (cf. Table 4). We have no conclusive explanation for the increased spread in Triton κ^{Θ}'s. Solubility is a necessary precondition for full expression of CCN activity, and solubility is low for weakly functionalized organic compounds [*Suda et al*., 2014]. Pure Triton is viscous and has low O:C ratio (~1:4), raising the possibility that Triton remains imperfectly mixed in the solution.

7. Summary and Conclusion

We studied the CCN activity of pure and internally mixed aerosols containing surfactants using scanning mobility CCN measurements. The assumption of surface tension reduction without accounting for bulk-to-surface partitioning resulted in several hundred percent overprediction of κ^{Θ}. Observed CCN activity of SDS was not enhanced relative to its hygroscopicity at subsaturated relative humidity. Observed CCN activity of Triton X-100 and Zonyl FS-300 was enhanced relative to molar volume predictions (equation (8)) [*Petters et al*., 2009a] and the partitioning model (Model 2) [*Raatikainen and Laaksonen*, 2011; *Petters and Kreidenweis*, 2013]. However, limiting surface adsorption to 1.5 monolayers resulted in better agreement between Model 2 and measurements, and we propose that models using partitioning theory add a constraining $\xi_{sft,min}$ that is tied to the maximum surface excess of surfactant as determined from the sorption isotherm. NaCl mixtures often consisted of nonspherical particles with derived dynamic shape factor ranging between 1 and 1.13. Unusually large scatter was observed for pure Triton X-100 and internal mixtures of Triton X-100 with ammonium sulfate and sodium chloride; the exact cause of which could not be determined. One possible explanation is fractionation of surfactant in spray atomizer. Generally, the shape of the mixing curves was not anticipated by ZSR mixing or by partitioning theory. A significant suppression of CCN activity relative to ZSR mixing or partitioning theory was observed at near equal volume mixing fractions, suggesting that solute-solute interactions may need to be considered when modeling mixed particles.

Acknowledgments
Access to all data supporting this work is detailed in the supporting information. This research was funded by the Department of Energy, Office of Biological and Environmental Sciences grants DE-SC 0010470 and DE-SC 0012043.

References

Álvarez-Silva, E., A. García-Abuín, D. Gómez-Díaz, J. M. Navaza, and I. Vidal-Tato (2010), Density, speed of sound, surface tension, and electrical conductivity of sodium dodecanoate aqueous solutions from $T = (293.15$ to $323.15)$ K, *J. Chem. Eng. Data*, *55*(9), 4058–4061, doi:10.1021/je100186x.

Andreae, M. O., and D. Rosenfeld (2008), Aerosol-cloud-precipitation interactions. Part 1. The nature and sources of cloud-active aerosols, *Earth Sci. Rev.*, *89*(1–2), 13–41, doi:10.1016/j.earscirev.2008.03.001.

Aumann, E., L. M. Hildemann, and A. Tabazadeh (2010), Measuring and modeling the composition and temperature-dependence of surface tension for organic solutions, *Atmos. Environ.*, *44*(3), 329–337, doi:10.1016/j.atmosenv.2009.10.033.

Baltensperger, U., et al. (2005), Secondary organic aerosols from anthropogenic and biogenic precursors, *Faraday Discuss.*, *130*, 265–278, doi:10.1039/B417367H.

Biskos, G., L. M. Russell, P. R. Buseck, and S. T. Martin (2006), Nanosize effect on the hygroscopic growth factor of aerosol particles, *Geophys. Res. Lett.*, *33* L07801, doi:10.1029/2005GL025199.

Brooks, S. D., P. J. DeMott, and S. M. Kreidenweis (2004), Water uptake by particles containing humic materials and mixtures of humic materials with ammonium sulfate, *Atmos. Environ.*, *38*(13), 1859–1868, doi:10.1016/j.atmosenv.2004.01.009.

Burrows, S. M., W. Elbert, M. G. Lawrence, and U. Pöschl (2009), Bacteria in the global atmosphere—Part 1: Review and synthesis of literature data for different ecosystems, *Atmos. Chem. Phys.*, *9*(23), 9263–9280, doi:10.5194/acp-9-9263-2009.

Campbell, A. N., and G. R. Lakshminarayanan (1965), Conductances and surface tensions of aqueous solutions of sodium decanoate, sodium laurate, and sodium myristate, at 25° and 35°, *Can. J. Chem.*, *43*(6), 1729–1737, doi:10.1139/v65-228.

Capel, P. D., R. Gunde, F. Zuercher, and W. Giger (1990), Carbon speciation and surface tension of fog, *Environ. Sci. Technol.*, *24*(5), 722–727, doi:10.1021/es00075a017.

Chan, M. N., and C. K. Chan (2003), Hygroscopic properties of two model Humic-like substances and their mixtures with inorganics of atmospheric importance, *Environ. Sci. Technol.*, *37*(22), 5109–5115, doi:10.1021/es034272o.

Christensen, S. I., and M. D. Petters (2012), The role of temperature in cloud droplet activation, *J. Phys. Chem. A*, *116*(39), 9706–9717, doi:10.1021/jp3064454.

Clegg, S. L., P. Brimblecombe, and A. S. Wexler (1998), Thermodynamic model of the system H^+–NH_4^+–Na^+–SO_4^{2-}–NO_3^-–Cl^-–H_2O at 298.15 K, *J. Phys. Chem. A*, *102*(12), 2155–2171, doi:10.1021/jp973043j.

Cui, Z., W. Fountain, M. Clark, M. Jay, and R. J. Mumper (2003), Novel ethanol-in-fluorocarbon microemulsions for topical genetic immunization, *Pharm. Res.*, *20*(1), 16–23, doi:10.1023/A:1022234305600.

Decesari, S., M. C. Facchini, S. Fuzzi, and E. Tagliavini (2000), Characterization of water-soluble organic compounds in atmospheric aerosol: A new approach, *J. Geophys. Res.*, *105*, 1481–1489, doi:10.1029/1999JD900950.

Decesari, S., M. C. Facchini, E. Matta, M. Mircea, S. Fuzzi, A. R. Chughtai, and D. M. Smith (2002), Water soluble organic compounds formed by oxidation of soot, *Atmos. Environ.*, *36*(11), 1827–1832, doi:10.1016/S1352-2310(02)00141-3.

Dinar, E., I. Taraniuk, E. R. Graber, S. Katsman, T. Moise, T. Anttila, T. F. Mentel, and Y. Rudich (2006), Cloud condensation nuclei properties of model and atmospheric HULIS, *Atmos. Chem. Phys.*, *6*(9), 2465–2482, doi:10.5194/acp-6-2465-2006.

Ekström, S., B. Nozière, and H. -C. Hansson (2009), The cloud condensation nuclei (CCN) properties of 2-methyltetrols and C3-C6 polyols from osmolality and surface tension measurements, *Atmos. Chem. Phys.*, *9*(3), 973–980, doi:10.5194/acp-9-973–2009.

Ekström, S., B. Nozière, M. Hultberg, T. Alsberg, J. Magnér, E. D. Nilsson, and P. Artaxo (2010), A possible role of ground-based microorganisms on cloud formation in the atmosphere, *Biogeosciences*, *7*(1), 387–394, doi:10.5194/bg-7-387-2010.

Engelhart, G. J., A. Asa-Awuku, A. Nenes, and S. N. Pandis (2008), CCN activity and droplet growth kinetics of fresh and aged monoterpene secondary organic aerosol, *Atmos. Chem. Phys.*, *8*(14), 3937–3949, doi:10.5194/acp-8-3937-2008.

Facchini, M. C., S. Decesari, M. Mircea, S. Fuzzi, and G. Loglio (2000), Surface tension of atmospheric wet aerosol and cloud/fog droplets in relation to their organic carbon content and chemical composition, *Atmos. Environ.*, *34*(28), 4853–4857, doi:10.1016/S1352-2310(00)00237-5.

Fors, E. O., et al. (2010), Hygroscopic properties of Amazonian biomass burning and European background HULIS and investigation of their effects on surface tension with two models linking H-TDMA to CCNC data, *Atmos. Chem. Phys.*, *10*(12), 5625–5639, doi:10.5194/acp-10-5625-2010.

Frosch, M., N. L. Prisle, M. Bilde, Z. Varga, and G. Kiss (2011), Joint effect of organic acids and inorganic salts on cloud droplet activation, *Atmos. Chem. Phys.*, *11*(8), 3895–3911, doi:10.5194/acp-11-3895-2011.

Ghyzel, P. J. (2013), Stabilized coating dispersions for porous inkjet recording media U.S. Patent 8,367,756, filed Dec. 27, 2007 and published Feb. 5, 2013.

Giordano, M. R., D. Z. Short, S. Hosseini, W. Lichtenberg, and A. Asa-Awuku (2013), Changes in droplet surface tension affect the observed hygroscopicity of photochemically aged biomass burning aerosol, *Environ. Sci. Technol.*, *47*(19), 10,980–10,986, doi:10.1021/es401867j.

Harmon, C. W., et al. (2010), Hygroscopic growth and deliquescence of NaCl nanoparticles mixed with surfactant SDS, *J. Phys. Chem. B*, *114*(7), 2435–2449, doi:10.1021/jp909661q.

Haynes, W. M. (2015), *CRC Handbook of Chemistry and Physics*, 95th ed., CRC Press, Boca Raton, Fla. [Available at http://www.hbcpnetbase.com. Accessed Feb. 17, 2015.]

Hinds, W. C. (1999), *Aerosol Technology: Properties, Behavior, and Measurement of Airborne Particles*, John Wiley, New York.

Ho, K. F., R. -J. Huang, K. Kawamura, E. Tachibana, S. C. Lee, S. S. H. Ho, T. Zhu, and L. Tian (2015), Dicarboxylic acids, ketocarboxylic acids, α-dicarbonyls, fatty acids and benzoic acid in $PM_{2.5}$ aerosol collected during CAREBeijing-2007: an effect of traffic restriction on air quality, *Atmos. Chem. Phys.*, *15*(6), 3111–3123, doi:10.5194/acp-15-3111-2015.

Hori, M., S. Ohta, N. Murao, and S. Yamagata (2003), Activation capability of water soluble organic substances as CCN, *J. Aerosol Sci.*, *34*(4), 419–448, doi:10.1016/S0021-8502(02)00190-8.

Irwin, M., N. Good, J. Crosier, T. W. Choularton, and G. McFiggans (2010), Reconciliation of measurements of hygroscopic growth and critical supersaturation of aerosol particles in central Germany, *Atmos. Chem. Phys.*, *10*(23), 11,737–11,752, doi:10.5194/acp-10-11737-2010.

Jackson, L. P., R. Andrade, I. Pleasent, and B. P. Grady (2014), Effects of pH and surfactant precipitation on surface tension and CMC determination of aqueous sodium n-alkyl carboxylate solutions, *J. Surfactants Deterg.*, *17*(5), 911–917, doi:10.1007/s11743-013-1528-3.

Kasper, G. (1982), Dynamics and measurement of smokes. I Size characterization of nonspherical particles, *Aerosol Sci. Technol.*, *1*(2), 187–199, doi:10.1080/02786828208958587.

King, S. M., T. Rosenoern, J. E. Shilling, Q. Chen, and S. T. Martin (2009), Increased cloud activation potential of secondary organic aerosol for atmospheric mass loadings, *Atmos. Chem. Phys.*, *9*(9), 2959–2971, doi:10.5194/acp-9-2959-2009.

Kiss, G., E. Tombácz, and H. Hansson (2005), Surface tension effects of humic-like substances in the aqueous extract of tropospheric fine aerosol, *J. Atmos. Chem.*, *50*(3), 279–294, doi:10.1007/s10874-005-5079-5.

Knutson, E. O., and K. T. Whitby (1975), Aerosol classification by electric mobility: Apparatus, theory, and applications, *J. Aerosol Sci.*, *6*(6), 443–451, doi:10.1016/0021-8502(75)90060-9.

Kreidenweis, S. M., K. Koehler, P. J. DeMott, A. J. Prenni, C. Carrico, and B. Ervens (2005), Water activity and activation diameters from hygroscopicity data—Part I: Theory and application to inorganic salts, *Atmos. Chem. Phys.*, *5*(5), 1357–1370, doi:10.5194/acp-5-1357-2005.

Kristensen, T. B., N. L. Prisle, and M. Bilde (2014), Cloud droplet activation of mixed model HULIS and NaCl particles: Experimental results and κ-Köhler theory, *Atmos. Res.*, *137*, 167–175, doi:10.1016/j.atmosres.2013.09.017.

Li, Z., A. L. Williams, and M. J. Rood (1998), Influence of soluble surfactant properties on the activation of aerosol particles containing inorganic solute, *J. Atmos. Sci.*, *55*(10), 1859–1866, doi:10.1175/1520-0469(1998)055<1859:IOSSPO>2.0.CO;2.

Lunkenheimer, K., W. Barzyk, R. Hirte, and R. Rudert (2003), Adsorption properties of soluble, surface-chemically pure *n*-alkanoic acids at the air/water interface and the relationship to insoluble monolayer and crystal structure properties, *Langmuir*, *19*(15), 6140–6150, doi:10.1021/la034379p.

MacMillan, A. C., J. B. Morrison, C. W. Harmon, and S. A. Nizkorodov (2012), Enhancement of surfactants in nanoparticles produced by an electrospray aerosol generator, *Aerosol Sci. Technol.*, *46*(11), 1239–1245, doi:10.1080/02786826.2012.708946.

Mikhailov, E., S. Vlasenko, S. T. Martin, T. Koop, and U. Pöschl (2009), Amorphous and crystalline aerosol particles interacting with water vapor: Conceptual framework and experimental evidence for restructuring, phase transitions and kinetic limitations, *Atmos. Chem. Phys.*, *9*(24), 9491–9522, doi:10.5194/acp-9-9491-2009.

21698996, 2016, 4, Downloaded from https://agupubs.onlinelibrary.wiley.com/doi/10.1002/2015JD024090 by University Of California, Wiley Online Library on [01/07/2024]. See the Terms and Conditions (https://onlinelibrary.wiley.com/terms-and-conditions) on Wiley Online Library for rules of use; OA articles are governed by the applicable Creative Commons License

Miller, R., P. Joos, and V. B. Fainerman (1994), Dynamic surface and interfacial tensions of surfactant and polymer solutions, *Adv. Colloid Interface Sci.*, *49*, 249–302, doi:10.1016/0001-8686(94)80017-0.

Mochida, M., N. Umemoto, K. Kawamura, H. Lim, and B. J. Turpin (2007), Bimodal size distributions of various organic acids and fatty acids in the marine atmosphere: Influence of anthropogenic aerosols, Asian dusts, and sea spray off the coast of East Asia, *J. Geophys. Res.*, *112* D15209, doi:10.1029/2006JD007773.

Moore, R. H., E. D. Ingall, A. Sorooshian, and A. Nenes (2008), Molar mass, surface tension, and droplet growth kinetics of marine organics from measurements of CCN activity, *Geophys. Res. Lett.*, *35* L07801, doi:10.1029/2008GL033350.

Nozière, B., C. Baduel, and J. Jaffrezo (2014), The dynamic surface tension of atmospheric aerosol surfactants reveals new aspects of cloud activation, *Nat. Commun.*, *5*, doi:10.1038/ncomms4335.

Padró, L. T., D. Tkacik, T. Lathem, C. J. Hennigan, A. P. Sullivan, R. J. Weber, L. G. Huey, and A. Nenes (2010), Investigation of cloud condensation nuclei properties and droplet growth kinetics of the water-soluble aerosol fraction in Mexico City, *J. Geophys. Res.*, *115* D09204, doi:10.1029/2009JD013195.

Petters, M. D., and S. M. Kreidenweis (2007), A single parameter representation of hygroscopic growth and cloud condensation nucleus activity, *Atmos. Chem. Phys.*, *7*(8), 1961–1971, doi:10.5194/acp-7-1961-2007.

Petters, M. D., and S. M. Kreidenweis (2013), A single parameter representation of hygroscopic growth and cloud condensation nucleus activity—Part 3: Including surfactant partitioning, *Atmos. Chem. Phys.*, *13*(2), 1081–1091, doi:10.5194/acp-13-1081-2013.

Petters, M. D., S. M. Kreidenweis, A. J. Prenni, R. C. Sullivan, C. M. Carrico, K. A. Koehler, and P. J. Ziemann (2009a), Role of molecular size in cloud droplet activation, *Geophys. Res. Lett.*, *36* L22801, doi:10.1029/2009GL040131.

Petters, M. D., C. M. Carrico, S. M. Kreidenweis, A. J. Prenni, P. J. DeMott, J. L. Collett Jr., and H. Moosmüller (2009b), Cloud condensation nucleation activity of biomass burning aerosol, *J. Geophys. Res.*, *114* D22205, doi:10.1029/2009JD012353.

Petters, M. D., H. Wex, C. M. Carrico, E. Hallbauer, A. Massling, G. R. McMeeking, L. Poulain, Z. Wu, S. M. Kreidenweis, and F. Stratmann (2009c), Towards closing the gap between hygroscopic growth and activation for secondary organic aerosol—Part 2: Theoretical approaches, *Atmos. Chem. Phys.*, *9*(12), 3999–4009, doi:10.5194/acp-9-3999-2009.

Petters, M. D., S. R. Suda, and S. I. Christensen (2013), The role of dynamic surface tension in cloud droplet activation, *AIP Conf. Proc.*, *1527*(1), 801–807, doi:10.1063/1.4803393.

Prausnitz, J. M., R. N. Lichtenthaler, and E. G. de Azevedo (1999), *Molecular Thermodynamics of Fluid-Phase Equilibria*, 3rd ed., Prentice Hall, Upper Saddle River, NJ.

Prisle, N. L., T. Raatikainen, R. Sorjamaa, B. Svenningsson, A. Laaksonen, and M. Bilde (2008), Surfactant partitioning in cloud droplet activation: A study of C8, C10, C12 and C14 normal fatty acid sodium salts, *Tellus: Ser. B*, *60*(3), 416–431, doi:10.1111/j.1600-0889.2008.00352.x.

Prisle, N. L., T. Raatikainen, A. Laaksonen, and M. Bilde (2010), Surfactants in cloud droplet activation: Mixed organic-inorganic particles, *Atmos. Chem. Phys.*, *10*(12), 5663–5683, doi:10.5194/acp-10-5663-2010.

Prisle, N. L., N. Ottosson, G. Öhrwall, J. Söderström, M. Dal Maso, and O. Björneholm (2012), Surface/bulk partitioning and acid/base speciation of aqueous decanoate: Direct observations and atmospheric implications, *Atmos. Chem. Phys.*, *12*(24), 12,227–12,242, doi:10.5194/acp-12-12227-2012.

Raatikainen, T., and A. Laaksonen (2011), A simplified treatment of surfactant effects on cloud drop activation, *Geosci. Model Dev.*, *4*(1), 107–116, doi:10.5194/gmd-4-107-2011.

Rehfeld, S. J. (1967), Adsorption of sodium dodecyl sulfate at various hydrocarbon-water interfaces, *J. Phys. Chem.*, *71*(3), 738–745, doi:10.1021/j100862a039.

Rood, M. J., and A. L. Williams (2001), Reply, *J. Atmos. Sci.*, *58*(11), 1468–1473, doi:10.1175/1520-0469(2001)058<1468:R>2.0.CO;2.

Rose, D., S. S. Gunthe, E. Mikhailov, G. P. Frank, U. Dusek, M. O. Andreae, and U. Pöschl (2008), Calibration and measurement uncertainties of a continuous-flow cloud condensation nuclei counter (DMT-CCNC): CCN activation of ammonium sulfate and sodium chloride aerosol particles in theory and experiment, *Atmos. Chem. Phys.*, *8*(5), 1153–1179, doi:10.5194/acp-8-1153-2008.

Ruehl, C. R., and K. R. Wilson (2014), Surface organic monolayers control the hygroscopic growth of submicrometer particles at high relative humidity, *J. Phys. Chem. A*, *118*(22), 3952–3966, doi:10.1021/jp502844g.

Ruehl, C. R., P. Y. Chuang, and A. Nenes (2010), Aerosol hygroscopicity at high (99 to 100%) relative humidities, *Atmos. Chem. Phys.*, *10*(3), 1329–1344, doi:10.5194/acp-10-1329-2010.

Russell, L. M., S. Zhang, R. C. Flagan, J. H. Seinfeld, M. R. Stolzenburg, and R. Caldow (1996), Radially classified aerosol detector for aircraft-based submicron aerosol measurements, *J. Atmos. Oceanic Technol.*, *13*(3), 598–609, doi:10.1175/1520-0426(1996)013<0598:RCADFA>2.0.CO;2.

Sattler, B., H. Puxbaum, and R. Psenner (2001), Bacterial growth in supercooled cloud droplets, *Geophys. Res. Lett.*, *28*, 239–242, doi:10.1029/2000GL011684.

Seidl, W., and G. Hänel (1983), Surface-active substances on rainwater and atmospheric particles, *Pure Appl. Geophys.*, *121*(5), 1077–1093, doi:10.1007/BF02590198.

Seinfeld, J. H., and S. N. Pandis (2006), *Atmospheric Chemistry and Physics: From Air Pollution to Climate Change*, John Wiley, Hoboken, N. J.

Shulman, M. L., M. C. Jacobson, R. J. Carlson, R. E. Synovec, and T. E. Young (1996), Dissolution behavior and surface tension effects of organic compounds in nucleating cloud droplets, *Geophys. Res. Lett.*, *23*, 277–280, doi:10.1029/95GL03810.

Škvarla, J., M. Uchman, K. Procházka, Z. Tošner, V. M. Garamus, S. Pispas, and M. Štěpánek (2014), Micellization of Zonyl FSN-100 fluorosurfactant in aqueous solutions, *Colloids Surf. A*, *443*, 209–215, doi:10.1016/j.colsurfa.2013.11.021.

Sorjamaa, R., B. Svenningsson, T. Raatikainen, S. Henning, M. Bilde, and A. Laaksonen (2004), The role of surfactants in Köhler theory reconsidered, *Atmos. Chem. Phys.*, *4*(8), 2107–2117, doi:10.5194/acp-4-2107-2004.

Spracklen, D. V., and C. L. Heald (2014), The contribution of fungal spores and bacteria to regional and global aerosol number and ice nucleation immersion freezing rates, *Atmos. Chem. Phys.*, *14*(17), 9051–9059, doi:10.5194/acp-14-9051-2014.

Suda, S. R., and M. D. Petters (2013), Accurate determination of aerosol activity coefficients at relative humidities up to 99% using the hygroscopicity tandem differential mobility analyzer technique, *Aerosol Sci. Technol.*, *47*(9), 991–1000, doi:10.1080/02786826.2013.807906.

Suda, S. R., M. D. Petters, A. Matsunaga, R. C. Sullivan, P. J. Ziemann, and S. M. Kreidenweis (2012), Hygroscopicity frequency distributions of secondary organic aerosols, *J. Geophys. Res.*, *117* D04207, doi:10.1029/2011JD016823.

Suda, S. R., et al. (2014), Influence of functional groups on organic aerosol cloud condensation nucleus activity, *Environ. Sci. Technol.*, *48*(17), 10,182–10,190, doi:10.1021/es502147y.

Sun, J., and P. A. Ariya (2006), Atmospheric organic and bio-aerosols as cloud condensation nuclei (CCN): A review, *Atmos. Environ.*, *40*(5), 795–820, doi:10.1016/j.atmosenv.2005.05.052.

Taraniuk, I., E. R. Graber, A. Kostinski, and Y. Rudich (2007), Surfactant properties of atmospheric and model humic-like substances (HULIS), *Geophys. Res. Lett.*, *34* L16807, doi:10.1029/2007GL029576.

21698996, 2016, 4, Downloaded from https://agupubs.onlinelibrary.wiley.com/doi/10.1002/2015JD024090 by University Of California, Wiley Online Library on [01/07/2024]. See the Terms and Conditions (https://onlinelibrary.wiley.com/terms-and-conditions) on Wiley Online Library for rules of use; OA articles are governed by the applicable Creative Commons License

Tuckermann, R. (2007), Surface tension of aqueous solutions of water-soluble organic and inorganic compounds, *Atmos. Environ.*, *41*(29), 6265–6275, doi:10.1016/j.atmosenv.2007.03.051.

Wagner, W., and A. Pruß (2002), The IAPWS formulation 1995 for the thermodynamic properties of ordinary water substance for general and scientific use, *J. Phys. Chem. Ref. Data*, *31*(2), 387–535, doi:10.1063/1.1461829.

Wang, S. C., and R. C. Flagan (1990), Scanning electrical mobility spectrometer, *Aerosol Sci. Technol.*, *13*(2), 230–240, doi:10.1080/02786829008959441.

Wang, Z., et al. (2010), The dynamic shape factor of sodium chloride nanoparticles as regulated by drying rate, *Aerosol Sci. Technol.*, *44*(11), 939–953, doi:10.1080/02786826.2010.503204.

Werner, J., J. Julin, M. Dalirian, N. L. Prisle, G. Öhrwall, I. Persson, O. Björneholm, and I. Riipinen (2014), Succinic acid in aqueous solution: Connecting microscopic surface composition and macroscopic surface tension, *Phys. Chem. Chem. Phys.*, *16*(39), 21,486–21,495, doi:10.1039/C4CP02776K.

Wex, H., T. Hennig, I. Salma, R. Ocskay, A. Kiselev, S. Henning, A. Massling, A. Wiedensohler, and F. Stratmann (2007), Hygroscopic growth and measured and modeled critical super-saturations of an atmospheric HULIS sample, *Geophys. Res. Lett.*, *34* L02818, doi:10.1029/2006GL028260.

Wex, H., M. D. Petters, C. M. Carrico, E. Hallbauer, A. Massling, G. R. McMeeking, L. Poulain, Z. Wu, S. M. Kreidenweis, and F. Stratmann (2009), Towards closing the gap between hygroscopic growth and activation for secondary organic aerosol: Part 1—Evidence from measurements, *Atmos. Chem. Phys.*, *9*(12), 3987–3997, doi:10.5194/acp-9-3987-2009.

Wexler, A. S. and S. L. Clegg (2002), Atmospheric aerosol models for systems including the ions H^+, NH_4^+, Na^+, SO_4^{2-}, NO_3^-, Cl^-, Br^-, and H_2O, *J. Geophys. Res.*, *107*(D14), 4207, doi:10.1029/2001JD000451.

Zdziennicka, A., K. Szymczyk, J. Krawczyk, and B. Jańczuk (2012), Activity and thermodynamic parameters of some surfactants adsorption at the water–air interface, *Fluid Phase Equilib.*, *318*, 25–33, doi:10.1016/j.fluid.2012.01.014.

Zelenyuk, A., Y. Cai, and D. Imre (2006), From agglomerates of spheres to irregularly shaped particles: Determination of dynamic shape factors from measurements of mobility and vacuum aerodynamic diameters, *Aerosol Sci. Technol.*, *40*(3), 197–217, doi:10.1080/02786820500529406.

Zhang, Y., and R. M. Miller (1992), Enhanced octadecane dispersion and biodegradation by a Pseudomonas rhamnolipid surfactant (biosurfactant), *Appl. Environ. Microbiol.*, *58*(10), 3276–3282.

21698996, 2016, 4, Downloaded from https://agupubs.onlinelibrary.wiley.com/doi/10.1002/2015JD024090 by University Of California, Wiley Online Library on [01/07/2024]. See the Terms and Conditions (https://onlinelibrary.wiley.com/terms-and-conditions) on Wiley Online Library for rules of use; OA articles are governed by the applicable Creative Commons License